Determining the Effect of Structure and Function on 3D Bioprinted Hydrogel Scaffolds for Applications in Tissue Engineering

by

Brent Godau
Bachelor of Science, University of Victoria, 2014

A Thesis Submitted in Partial Fulfillment
of the Requirements for the Degree of

Master of Applied Science

in the Department of Mechanical Engineering

Supervisory Committee

Determining the Effect of Structure and Function on 3D Bioprinted Hydrogel Scaffolds for Applications in Tissue Engineering

by

Brent Godau
BSc, University of Victoria, 2014

Supervisory Committee

Dr. Mohsen Akbari, Mechanical Engineering
Supervisor

Dr. Keivan Ahmadi, Mechanical Engineering
Departmental Member

Abstract

The field of tissue engineering has grown immensely since its inception in the late 1980s. However, currently commercialized tissue engineered products are simple in structure. This is due to a pre-clinical bottleneck in which complex tissues are unable to be fabricated. 3D bioprinting has become a versatile tool in engineering complex tissues and offers a solution to this bottleneck. Characterizing the mechanical properties of engineered tissue constructs provides powerful insight into the viability of engineered tissues for their desired application. Current methods of mechanical characterization of soft hydrogel materials used in tissue engineering destroy the sample and ignore the effect of 3D bioprinting on the overall mechanical properties of a construct. Herein, this work reports on the novel use of a non-destructive method of viscoelastic analysis to demonstrate the influence of 3D bioprinting strategy on mechanical properties of hydrogel tissue scaffolds. 3D bioprinting is demonstrated as a versatile tool with the ability to control mechanical and physical properties. Structure-function relationships are developed for common 3D bioprinting parameters such as printed fiber size, printed scaffold pattern, and bioink formulation. Further studies include effective real-time monitoring of crosslinking, and mechanical characterization of multi-material scaffolds. We envision this method of characterization opening a new wave of understanding and strategy in tissue engineering.

Table of Contents

List of Tables

List of Figures

Acknowledgments

I would like to thank Dr. Mohsen Akbari for his guidance and mentorship throughout my time in the Laboratory for Innovations in MicroEngineering. Without his insight and contagious enthusiasm within the field of biomaterials and tissue engineering, this thesis would not have been possible. I will always be grateful for the opportunities he has provided me.

I would like to thank Dr. Anis Hadj Henni and Dr. Cedric Schmitt of Rheolution Instruments. The opportunity they provided me with industrial collaboration and dedicated involvement in this project was invaluable for my professional development.

I would like to thank Dr. Caterina Valeo for the use of her facilities for a large portion of this project.

I would like to acknowledge my fellow lab members for their ongoing support and shared experience in the lab. Without the professional relationships and friendships developed throughout this project, the experience would have been a lot less fun. I wish them all the best of luck in their endeavors.

Lastly, my sincere gratitude goes out to my parents, sister and brother-in-law, and girlfriend. Without their unwavering love and support, I would not have had the same opportunities and accomplishments I have today.

Dedication

I would like to dedicate this thesis to my grandparents. Nana & Opa, I thank you for instilling a passion for learning and education in me. Grampa Herk and Nanny Lucille, I thank you for your sense of humour and familial values. Grampa Sandy and Nanny Lyons, I thank you for teaching me to have fun in life. The values you all instilled in my parents have been passed down to me and made me the person I am today.

Disclaimer

This project was funded by the Natural Sciences and Engineering Research Council Engage grant program. The program promotes collaboration between industry and academia. For this specific project, funding, in-kind support, and consultation was provided by Rheolution, Inc.

Introduction

Human tissues and organs can lose their ability to properly function due to age, disease, damage, or congenital defects (Barr, Rodger and Kelly, 2019). Regenerative medicine is the branch of medicine focused on repairing, replacing, or regenerating injured or damaged cells, tissues, or organs. This includes cell therapies, gene therapies, tissue engineering, and more. The term "tissue engineering," first coined in 1993, refers to the interdisciplinary field in which the principles of engineering and the life sciences are used to develop biological substitutes capable of restoring, maintaining, or improving tissue function in the body (Langer and Vacanti, 1993). General strategies in tissue engineering include the use of cells alone as a therapy to regenerate injured tissue, the use of biomaterials and/or drugs and growth factors to induce tissue regeneration, and the use of biomaterial scaffolds with cells encapsulated or seeded onto the scaffold. Strategies including cells are often grown *in vitro* before implantation in the body or use as a model for pharmaceutical testing or improved understanding of biological and disease processes (Olson, Atala and Yoo, 2011).

Over the past thirty years, significant progress has been made in tissue engineering, and the economic history and outlook suggests that the regenerative medicine industry will have a great impact in health and medicine. By the end of 2018, The Alliance for Regenerative Medicine, a global advocate for regenerative medicine, reported that more than 906 companies were operating in the regenerative medicine industry (*Annual Regenerative Medicine Data Report*, 2018). This accounts for gene therapies, cell therapies, and tissue engineering therapies. Globally, $13.3 billion USD in financing was raised by regenerative medicine companies with $936.9 million USD raised by companies

operating within the tissue engineering sector, accounting for a 258% increase in financing over 2017. A recent study by Kim *et al*., which reviewed the tissue engineering and cell therapy market in the United states from 2011 to 2018, classified three categories of companies operating commercially in the industry by their products: biomaterials based, cells and biomaterials based, and stem cell based (Kim *et al.*, 2018). The sales generated by tissue engineering and cell therapy products from companies in the study estimated $9 billion USD in 2017, with approximately 99% of sales contributed from biomaterials-based products, ~1% contributed from cells and biomaterials-based products, and <1% contributed from stem cell based products.

This brief economic analysis suggests that cell therapy companies are generating more investment than engineered tissue therapies by a high margin, however, engineered tissue therapies which include biomaterials are generating more commercial sales comparatively. A simple Google Scholar search of the terms “tissue engineering,” “cell therapy,” and “regenerative medicine” outputs 1.46 million, 860,000, and 809,000 search results, respectively, suggesting that the field of tissue engineering is widely researched and receiving a lot of funding. This idea is supported by increasing and sustained impact factors of popular tissue engineering journals shown in Figure 0-1 (Clarivate Analytics, 2019b, 2019a, 2019c). With plenty of research and notable sales after commercialization, one would expect that the amount of financing in tissue engineered products might be comparable to cell therapies considering they require similar materials and methods of production. The evidence suggests that there is a bottleneck somewhere in the process of translating an engineered tissue from the research phase to commercialization.

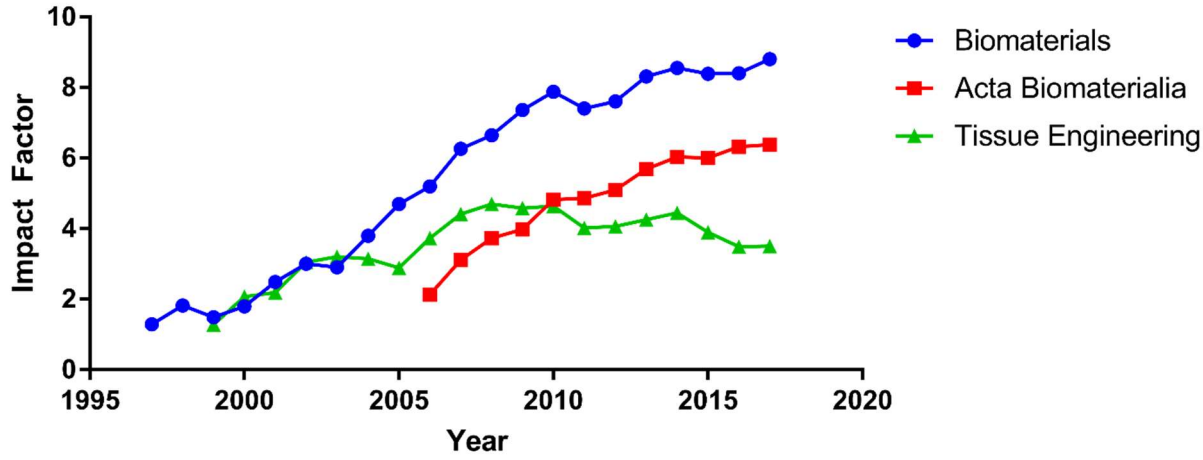

Figure 0-1 Impact factor of three popular journals in the field of tissue engineering over the past 25 years.

It is common understanding in the pharmaceutical industry that clinical translation from the drug discovery and development phase employs a bottleneck on the majority of drugs with only 10.4% of drugs in phase I clinical trials moving to further stages (Hay *et al.*, 2014). It should be expected that a similar bottleneck effect will happen with regenerative medicine therapies in which manipulation of human biology is being conducted, however, tissue engineering received 7% of the total financial investment in regenerative medicine in 2018 while accounting for only 4% of the total number of clinical trials, signifying decent translation from clinical trials to commercialization (*Annual Regenerative Medicine Data Report*, 2018). The evidence suggests that there may also be a substantial bottleneck before translating an engineered tissue therapy to clinical trials.

Interestingly, evidence for a pre-clinical bottleneck in commercialization of engineered tissue products arises in the products that have made it through the process of

commercialization. For example, Apligraf, a tissue engineered skin substitute consisting of both a biomaterial scaffold and human cells used for treating burns and diabetic ulcers, was the first tissue engineered product to reach commercialization (Parenteau, 1999). Other examples of successful products include tissue engineered cornea, urethra, urinary bladder, and blood vessels (Atala, Kurtis Kasper and Mikos, 2012). Similarities in these products are that they are planar or hollow structures, often comprised of layered tissue or cell types. This simplicity in structure is a much more attainable goal with regard to many aspects of tissue engineering (see Figure 0-2), manufacturing, supply chain management, and regulation.

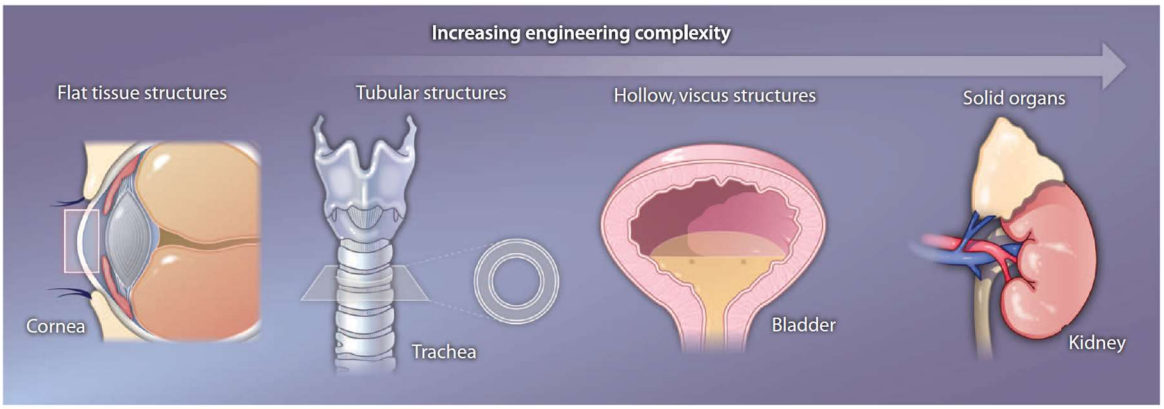

Figure 0-2 Increasing complexity of tissues in the human body. From (Atala, Kurtis Kasper and Mikos, 2012). Reprinted with permission from AAAS.

When attempting to engineer more complex tissues and organs, challenges arise in the following areas:

1. Supplying nutrients and oxygen to cells embedded within a tissue via formation of complex vasculature
2. Complex spatial arrangement of multiple cell types

3. Attaining suitable mechanical strength and substrate stiffness for tissue- and cell-specific requirements
4. Incorporation of the engineered tissue product into the native tissue environment after implantation

(Foyt *et al.*, 2018). Furthermore, manufacturing with consideration of good manufacturing practice, sterility and purity of the product, quality control, and scalability present great challenges (Atala, Kurtis Kasper and Mikos, 2012). Undoubtedly, there will not be a simple fix to these incredibly complex challenges at the interface of engineering, medicine, biology, and chemistry. However, an enabling technology, three-dimensional (3D) bioprinting, offers an array of solutions to some of the most challenging contributors delaying major progress in tissue engineering.

3D printing, used interchangeably with additive manufacturing, is a method of fabrication in which 3D structures are built by depositing material onto a substrate layer-by-layer (Murphy and Atala, 2014). 3D bioprinting applies this same technique, but uses biocompatible materials, cells, and supporting components for applications in regenerative medicine, biotechnology, and pharmaceuticals. This technique is advantageous in the field of tissue engineering for its ability to spatially arrange multiple cell types, biomolecules, and biomaterials to engineer tissue with similar arrangement and complexity to the native tissue. Furthermore, 3D bioprinting is a computer assisted technology, allowing for tissue generation in a mechanized, organized, and optimized manner (Lee and Yeong, 2016). Considering that 3D printing is traditionally a technique developed for fabrication of molten plastics and metals, significant research and development has gone into adapting

and innovating this technology for use with sensitive, living biological materials (Murphy and Atala, 2014). This has spawned an entire industry of commercially available 3D bioprinters and associated products with over 17 leading companies operating across the globe (Pereira *et al.*, 2018).

With major innovations in 3D bioprinting and widespread use of the technique for tissue engineering, there is a need for improved understanding of how 3D bioprinting strategy can be employed to optimize engineered tissues (Khademhosseini and Langer, 2016; Kelly *et al.*, 2018). Common practice in development of engineered tissue is to characterize the components of the engineered tissue for their desired function individually and, once the engineered tissue is biofabricated, as a complete structure. The major deciding factor, apart from significant medical and economic feasibility, for an engineered tissue to move on to animal testing and, ideally, progress forward to clinical trials is the success and thoroughness of the *in vitro* testing. Typical *in vitro* assessment of scaffolds for tissue engineering addresses criteria based on biocompatibility, biodegradability, mechanical properties, scaffold architecture, and manufacturing technology (O'Brien, 2011). Conveniently, the adjustable parameters in 3D bioprinting have direct influence over these criteria, deeming it a formidable tool in tissue engineering (Khademhosseini and Langer, 2016; Kelly *et al.*, 2018). However, an incomplete understanding of how 3D bioprinting parameters have direct influence over these criteria limits effective optimization of 3D bioprinted constructs for tissue engineering (Zadpoor, 2017; Kelly *et al.*, 2018).

This lack of understanding, particularly in the effect of changes in 3D bioprinted architecture on the mechanics and physical properties of biomaterial scaffolds for tissue

engineering, is partly due to the inability to effectively characterize this effect (Hollister, 2005; Jakus, Rutz and Shah, 2016). A Canadian company, Rheolution Instruments, based out of Montreal has developed a new method of analyzing the viscoelastic properties of soft materials used in tissue engineering applications (*Rheolution Inc. - Soft Materials Testing Instruments*, 2019). Their method of analysis, viscoelastic testing of bilayered materials (VeTBiM), has previously been shown to be effective for non-destructive and contactless characterization of bulk hydrogel materials (Ceccaldi *et al.*, 2017). Hydrogels are gels with networks of hydrophilic polymers capable of absorbing high amounts of water. The ElastoSens Bio2, an instrument made by Rheolution, has been designed for use in biomaterials labs and lends itself as a platform for developing relationships between the structure and function of 3D bioprinted scaffolds for tissue engineering.

This thesis addresses fundamental understanding of how 3D printing strategy can be employed and optimized to engineer complex tissue. A novel method using technology made by Rheolution Instruments is used to characterize the effect of 3D bioprinting on hydrogel scaffolds mechanical and physical properties. By addressing this understanding, more effective use of 3D bioprinting technology can be made, reducing the inability to engineer complex tissues. First, an overview of the field of 3D bioprinting and the strategy involved in engineering tissue will be discussed. Moving forward, methods of mechanical characterization of biomaterials in tissue engineering applications will be discussed and compared to the technology developed by Rheolution Instruments. Finally, the developed method of characterization and relationships between structure and function of 3D bioprinted scaffolds will be detailed with support from primary data.

Chapter 1 3D Bioprinting: Concept, Strategy, and Characterization

3D bioprinting is "the use of material transfer processes for patterning and assembling biologically relevant materials/molecules, cells, tissues, and biodegradable biomaterials with a prescribed organization to accomplish one or more biological functions" (Mironov, Reis and Derby, 2006). In the late 1980s, the advent of both tissue engineering and additive manufacturing, also known as 3D printing, started two separate research fields that would both individually revolutionize the fields of medicine and engineering, respectively (Hull, 1984; Vacanti, 2006). Over the past 20 years, 3D printing contributed many significant advances in manufacturing, aerospace, consumer products, arts, and the food industry (Zhu *et al.*, 2016). Significant advancements were made in tissue engineering throughout the 1990s, however, the amalgamation of 3D printing techniques and tissue engineering have spawned a thriving industry of 3D bioprinting, presenting itself as an effective biofabrication technique with solutions to many of the major challenges imposed in the field of tissue engineering (Jose *et al.*, 2016). As mentioned in the introduction, major challenges lie within engineering tissues that are comparable in complexity to native tissue structure. 3D bioprinting is believed to be capable of offering unprecedented versatility in delivering cells and biomaterials with accurate control over spatial distribution, thus bridging the disparity between artificially engineered tissue and native tissue (Zhang *et al.*, 2017). This versatility enables the formation of complex architectures, shapes, and features that influence the overall tissue function, also allowing for potential patient personalization.

There are three central approaches to engineering tissues in 3D bioprinting: biomimicry, autonomous self-assembly, and mini-tissue assembly (Murphy and Atala, 2014). In biomimicry, the target tissue is studied, and the native micro- and macro- architecture is fabricated with the goal of mimicking the native tissue using suitable biomaterials. Strategies in material selection, material processing, mechanical properties, and structural properties can be employed to mimic the native tissue extracellular matrix (ECM). Further consideration in cell type(s), drugs and growth factors, and tissue culture strategy play an important role in tissue growth and maturation. Autonomous self assembly draws inspiration from natural embryonic growth to develop tissues. Natural tissue development and growth is an autonomous process regulated by cell signalling, cellular production of ECM to generate the necessary tissue microstructure and function, and other physical and chemical cues to guide cellular differentiation to the target tissue. This strategy can be conducted with or without a scaffold and relies on the cells and environment to guide tissue or organ development. Finally, mini-tissue assembly uses the concept of having mini functional tissue building blocks which can be fabricated and later assembled into a larger tissue or organ structure. This process relies both on biomimicry and, in some cases, autonomous self assembly to assemble multiple mini tissues into a larger tissue. All three of these strategies involve a general 3D bioprinting process which consists of imaging the patient tissue, designing the engineered tissue, material and cell selection, and bioprinting (see Figure 1-1).

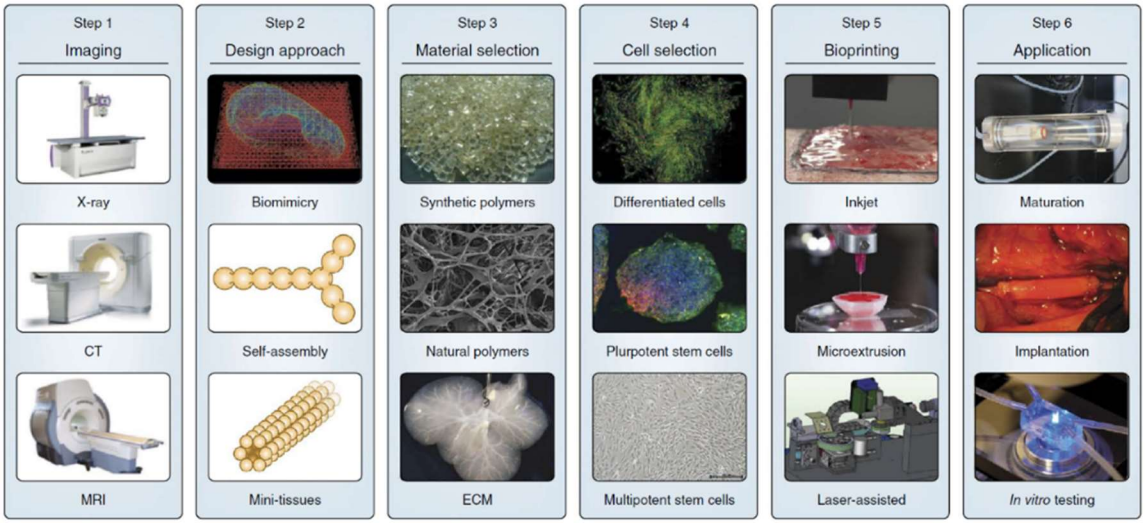

Figure 1-1 The overall process of 3D bioprinting: (1) the desired tissue or organ can be imaged to prepare a design; (2) selection of tissue fabrication approach; (3) selection of bioink material; (4) selection of cell types; (5) selection of bioprinting technique; (6) employ the tissue for use in its intended application. Reprinted with permission from Springer Nature (Murphy and Atala, 2014).

The purpose of this chapter is to discuss the field of 3D bioprinting and how the technique can be employed to optimize engineered tissues. First, the different types of 3D bioprinting will be discussed, followed by a brief review of hydrogel bioinks for 3D printing applications. Subsequently, strategy in 3D printed scaffold design and its influence on engineered tissue constructs will be explored. Finally, methods of characterizing 3D bioprinted structures will be discussed.

1.1 Types of 3D Bioprinting

Both the terms 3D printing and 3D bioprinting have evolved to encompass many techniques of additive manufacturing, with the latter referring to techniques involving biomaterials and cells for medical and biotech applications (Pedde *et al.*, 2017). In the world of 3D printing, widely employed practices include techniques that fuse solid

materials and powders on the print bed by either binding agent or directed energy deposition, techniques that employ fused deposition of thermoplastics, and photopolymerization of liquid resin in a vat using a laser or projected light (also known as stereolithography). For 3D bioprinting, working with biocompatible materials limits the techniques to using materials that have high water content and can be deposited and/or crosslinked. Due to this material limitation, 3D bioprinting techniques typically use materials that are in a liquid or gel state. Crosslinking provides a chemical link between polymer chains in order to improve structural rigidity of the 3D bioprinted constructs. The four main 3D bioprinting techniques that are compatible with the material requirements and will be further discussed in this section are: inkjet bioprinting, microextrusion bioprinting, laser assisted bioprinting (LAB), and stereolithographic bioprinting.

1.1.1 Inkjet Bioprinting

The ability of inkjet technology for printing biological materials was first demonstrated by Klebe *et al.* in 1987 when he printed a solution of two ECM proteins, collagen and fibronectin, onto a substrate for subsequent seeding of cells in a two dimensional pattern (Klebe, 1988). This technique was further translated to inkjet-based 3D bioprinting in 2003 using a modified Hewlett-Packard printer as a proof-of-concept (Wilson and Boland, 2003). Inkjet bioprinting, adapted from conventional inkjet printing used for desktop printers, dispenses droplets of liquid solutions onto the printbed driven by thermal, piezoelectric, or microvalve processes (see Figure 1-2) (Gudapati, Dey and Ozbolat, 2016; Rider *et al.*, 2018). The droplets of solution can be positioned in a highly precise manner

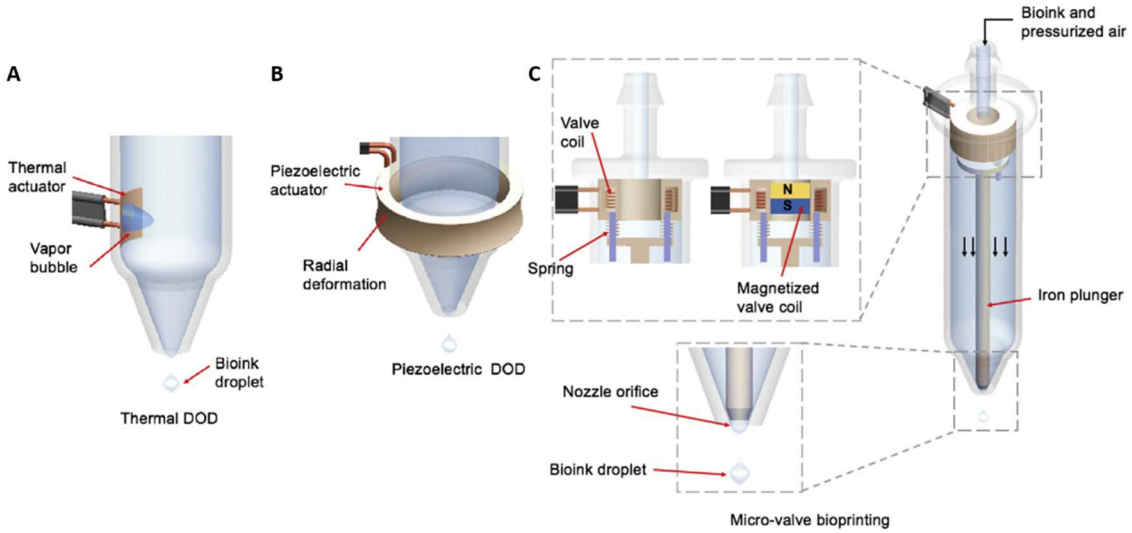

Figure 1-2 Methods of inkjet bioprinting. (A) thermally actuated inkjet printing deposits droplets by forming a vapour bubble. (B) Piezoelectrically actuated inkjet printing forms droplets with radial deformation. (C) Microvalve inkjet printing pressurizes the bioink and opens a valve to deposit droplets. Reprinted with permission from Elsevier (Gudapati, Dey and Ozbolat, 2016).

at a high speed, allowing for the construction of complex 3D structures and irregular shapes. After deposition, the constructs are polymerized with chemical, ionic, ultraviolet, or enzymatic crosslinking to fuse the deposited material into a gel-like construct (Pedde *et al.*, 2017).

Inkjet bioprinting offers some distinct advantages, such as high printing speeds of up to 10,000 droplets per second, moderately high resolution suitable for biological constructs (on the order of 50-300 μm), low cost, and control of the concentration gradient of cells and growth factors in materials. Interestingly, a common strategy to employ inkjet bioprinting is to convert a commercially available inkjet printer to work with biomaterials, contributing to the cost-effectiveness of this technique (Cui *et al.*, 2014). As with any biofabrication techniques, there are some associated limitations. For example, the liquid

phase requirement for inkjet printing limits the viscosity range of printable materials to 3.5-12 mPa·s, preventing effective fabrication of thicker vertical structures (Murphy and Atala, 2014). Furthermore, encapsulated cells in solution have an increasing effect on the viscosity of the solution, limiting the density of encapsulated cells in solution. Due to this limitation, fabrication of thick complex tissues poses a great challenge. Therefore, this technique may best be suited to the strategies of using mini-tissues and autonomous self-assembly to create larger, complex tissues.

1.1.2 Microextrusion Bioprinting

Microextrusion bioprinting is the 3D bioprinting alternative to the traditional 3D printing technique of fused deposition modeling (FDM) in which a biomaterial is continuously extruded through a needle or nozzle to deposit filaments or fibers on a substrate (Pedde *et al.*, 2017). First employed in the early 2000s, microextrusion bioprinting has become the most common form of 3D bioprinting for its affordability and versatility (Murphy and Atala, 2014; Pedde *et al.*, 2017). The filaments or fibers are extruded mechanically with the use of a pneumatic pump, piston, or screw to drive fluid flow and built up, layer-by-layer, into a 3D structure using a robotic stage and printhead capable of XYZ directional mobility (Ning and Chen, 2017). Microextrusion bioprinting typically uses soft biomaterials in the form of a hydrogel, such as natural or synthetic polymers. Much like inkjet bioprinting, the materials can be crosslinked ionically, enzymatically, chemically, or with ultraviolet light, however, they can also be crosslinked thermally (Pedde *et al.*, 2017). The resolution of the printed fibers is dependent on a number of factors: the size of the needle or nozzle used, the flow rate of the extruded material (or applied pressure), and the

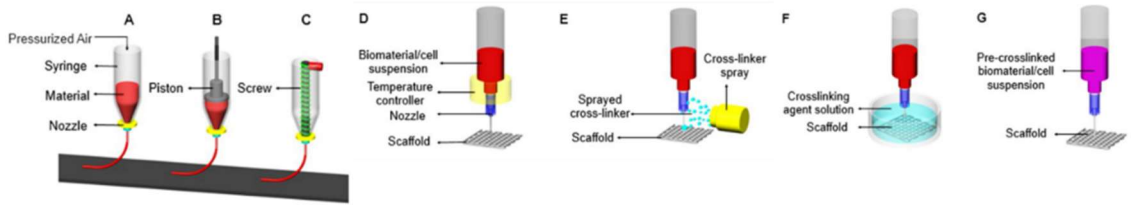

Figure 1-3 Summary of microextrusion methods: (A) pneumatic, (B) piston-based, and (C) screw-based extrusion. Summary of microextrusion bioprinting crosslinking methods: (D) thermal (E) crosslinking solution spray, (F) crosslinking bath, and (G) pre-crosslinked bioink. Reprinted with permission from John Wiley and Sons, Inc. (Ning and Chen, 2017).

speed of the printhead while dispensing material. Crosslinking can occur throughout varying parts of the process. For example, pre-crosslinking of material with limited amount of crosslinker before 3D printing can be used to improve the stability of printed structures, spraying crosslinker solution during or shortly after deposition of materials solidifies structures before they spread on the substrate, or printing directly into a crosslinking bath is often employed (see Figure 1-3) (Ning and Chen, 2017). As mentioned previously, materials can be thermally crosslinked with the addition of a temperature-controlled print cartridge to reduce material viscosity for deposition. Thermally sensitive polymers will alter their viscosity with changes in temperature. Furthermore, the use of shear-thinning biomaterials, which reduce their viscosity when exposed to shear stress, are compatible with this technique and may be used with or without crosslinking (Pedde *et al.*, 2017).

The main advantages of microextrusion bioprinting are related to the versatility of the technique. The use of mechanical force to dispense materials and adjustable nozzle or needle inner diameter enables a high working range of material viscosities (30 mPa·s to >600 kPa·s) and the ability to print a high concentration of cells or cell aggregates similar to the numbers of cells seen in natural tissues (Malda *et al.*, 2013; Pedde *et al.*, 2017).

Furthermore, higher material viscosity and a variety of crosslinking methods to choose from allow for high printed fiber fidelity and the construction of tall vertical structures (Pedde *et al.*, 2017). The resolution can vary from low to high, however, it is a trade off between a few factors. Higher resolution requires a smaller nozzle diameter and imposes higher shear stress on the material, requiring higher pressure to extrude the material and, if cells are encapsulated in the material, reducing cell viability. Depending on the design of the printed structure, lower resolution structures may be satisfactory and will maintain a higher encapsulated cell viability. Other challenges with this technique include nozzle clogging and insufficient interlayer bonding depending on the crosslinking method. Despite these minor challenges, microextrusion bioprinting enables fabrication of constructs in clinically relevant sizes and is often regarded as the most promising technique of bioprinting (Derby, 2012; Ferris *et al.*, 2013).

1.1.3 Laser Assisted Bioprinting

Laser assisted bioprinting, the bioprinting alternative to laser induced forward transfer (LIFT), relies on the use of a donor slide of biomaterial covered with a laser energy absorbing layer which locally evaporates and projects the donor slide material onto the substrate (see Figure 1-4) (Catros *et al.*, 2011). LIFT was originally developed for patterning inorganic materials and metals onto a substrate, but was demonstrated to be effective in depositing biological materials in 1999 by Odde and Renn (Odde and Renn, 1999; Chrisey, McGill and Pique, 2000). This nozzle-free (and clog free) approach has a major benefit in that it is able to deposit biomaterials containing high cell densities while maintaining high cell viability and resolution of the deposited droplets (Malda *et al.*, 2013).

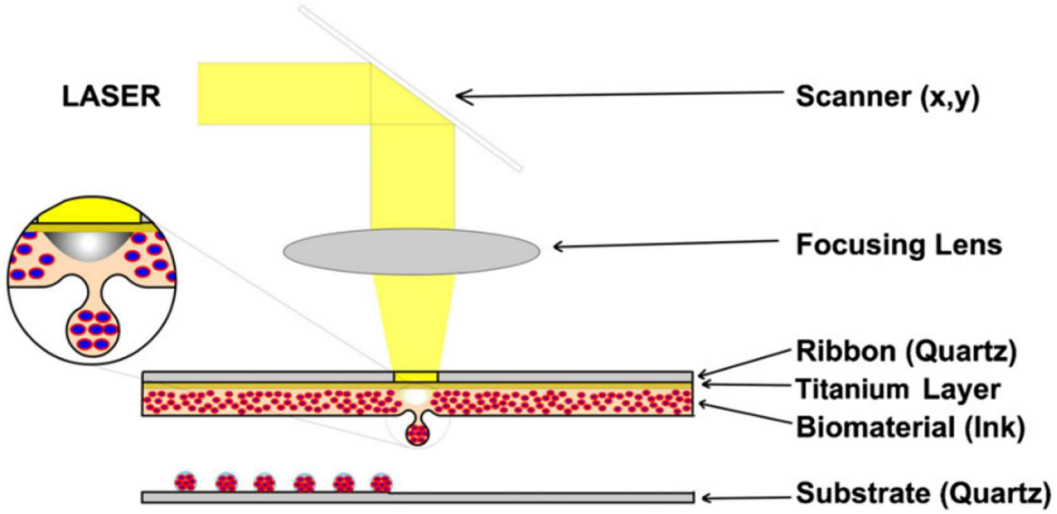

Figure 1-4 Laser assisted bioprinting diagram. Absorbed laser energy on the ribbon and titanium (energy absorbing layer) causes a bubble to form and project biomaterial in the donor slide onto the substrate. © IOP Publishing. Reproduced with permission. All rights reserved (Catros *et al.*, 2011).

The resolution is such that single cells can be dispensed in a droplet 20-80 µm in diameter (Pedde *et al.*, 2017). In order for laser assisted bioprinting to be employed, the material is required to be moderately low in viscosity (1-300mPa·s) and have a fast gelation mechanism to achieve high shape fidelity of 3D bioprinted constructs (Murphy and Atala, 2014). Furthermore, preparation of donor slides is time-consuming and challenging for printing multiple materials or cell types. These technical limitations, along with the high cost of laser sources, inhibit the generation of clinically relevant 3D constructs and widespread use of the technique (Malda *et al.*, 2013; Pedde *et al.*, 2017).

1.1.4 Stereolithographic Bioprinting

Stereolithography is another nozzle free technique in which a bath of photo-crosslinkable material, or resin, is irradiated either by a rastering laser or patterned UV light with a digital micromirror device (DMD) (see Figure 1-5) (Pedde *et al.*, 2017; Miri *et al.*, 2018). Exposure to the light source crosslinks the material, allowing for layer-by-layer construction of thick, complex 3D structures. Stereolithographic printers which use DMDs allow for very rapid fabrication of complex structures with unparalleled resolution on the order of 6 µm (Soman *et al.*, 2013). Furthermore, stereographically printed structures exhibit strong interlayer bonding, which is a pitfall in all three of the other 3D bioprinting methods (Pedde *et al.*, 2017). Due to the nature of this technique, the only method of crosslinking is photo-induced, which requires the addition of photo-initiating chemicals to

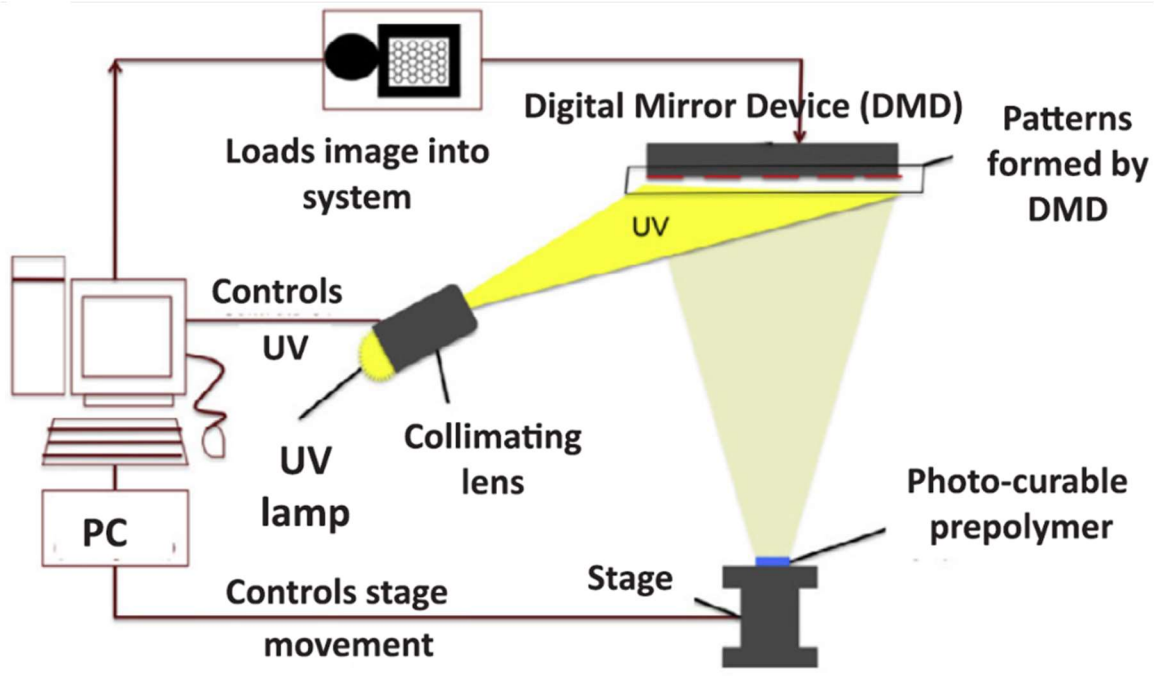

Figure 1-5 An example of a stereolithographic 3D printer with a DMD to project light onto the sample stage. Reprinted from with permission from (Miri *et al.*, 2018) Elsevier.

induce crosslinking of macromers via the formation of free radicals in solution (Rider *et al.*, 2018). Unfortunately, commonly used photo-initiating chemicals (eg. Irgacure 2959 and eosin Y) and UV light can be detrimental to cell viability due to their interference with cell growth and proliferation signalling pathways (Xu *et al.*, 2015). This requires fine-tuning of both the photo-initiator concentration and UV light exposure time so that effective crosslinking can be achieved while minimizing harmful effects on cells encapsulated in the biomaterial. Material limitations of this method require a viscosity of <5 Pa·s and the ability to be photo-crosslinked, narrowing the variety of printable materials for tissue engineering applications to either modified natural polymers or synthetic polymers. Furthermore, the requirement of a bath of material for printing limits the material to only one cell type or formulation, preventing the formation of complex tissues with multiple cell types or regions containing different biomolecules.

1.2 Bioinks

One part of the tissue engineering process, material selection and development, is becoming a widely studied field of research. Two pioneers in the field of tissue engineering, Dr. Robert Langer and Dr. Ali Khademhosseini, consider the development of improved biomaterials that enable fabrication of improved biomimetic tissues to be one of the attributing factors to the growth of the field of tissue engineering (Khademhosseini and Langer, 2016). This attribution is in part due to the development of new bioinks, or, by definition, the fluids that 3D bioprinters deposit (Whitford and Hoying, 2016). It should be noted that recent discussion in the field draws distinction between bioinks for different functions (structural, functional, sacrificial, cell-laden, etc.) in tissue engineering, however,

for the purposes of this thesis, the abovementioned definition will be used (Groll *et al.*, 2018; Williams *et al.*, 2018). In this section, the properties of bioinks will be discussed, followed by traditional polymers widely used for bioinks, and, finally, a brief discussion about advanced bioinks which are propelling the advancement of 3D bioprinting.

1.2.1 Bioink Properties

The development of improved bioinks is centered around a set of criteria that considers both the biofabrication process and development of the engineered tissue for its desired application. With regard to the biofabrication process, the rheological properties of the bioink and the method of gelation or crosslinking have direct influence over the print fidelity of the 3D bioprinted construct (Malda *et al.*, 2013). Rheology, or the study of the flow of matter under application of an external force, relates to fluid properties such as viscosity, shear thinning behaviour, and yield stress. The viscosity, or resistance of a fluid to flow, is important for print fidelity because it will ensure that extruded bioink forms fibers instead of droplets and that the deposited fibers will not spread on the substrate. An increased viscosity is correlated with increased polymer concentration in solution and increased molecular weight of the polymer. However, with increasing viscosity, increased force is required to extrude the bioink through a nozzle or needle, thus increasing the shear forces within the fluid. This is not a desirable effect if cells are encapsulated in the bioink and can increase the likelihood of material clogging. Shear thinning capability of a bioink, in which the viscosity of the bioink decreases when shear stress is applied, is a partial remedy to this issue. This non-Newtonian fluid behaviour is the result of reorganization of polymer chains in solution when shear stress is applied and is often a property present in

polymeric solutions. Shear thinning behaviour is desirable for 3D bioprinting because it reduces the force required to extrude material and, if cells are encapsulated, reduces exposure to shear stress.

Yield stress is the force that must be overcome to initiate fluid flow. This resistance to fluid flow is the result of physical interactions between molecular chains in solutions, and once enough force has been provided to break these interactions, the fluid will flow with less force applied. After fluid flow stops, the physical interactions will slowly recover and prevent the collapse of the deposited structure. Sufficient yield stress is desirable for print fidelity, but too high can make the printing process more difficult. Finally, suitable gelation time and crosslinking mechanism must allow for an efficient biofabrication process that can be completed in a short time frame to keep cells viable outside of a nutrient rich environment (Gopinathan and Noh, 2018).

Aside from bioink properties that are useful for the biofabrication process, a bioink must exhibit beneficial properties that support the effective growth of and maturation of an engineered tissue. This includes a suitable micro-architecture that can mimic the native microenvironment of the native tissue and allow for cell attachment to cell specific binding sites without overcrowding or too much distance between neighbouring cells (Williams *et al.*, 2018). The mechanical stiffness of the bioink should match the native tissue ECM in order to optimize differentiation, proliferation, and gene expression of cells (Williams, 2014). The bioink should be non-cytotoxic, non-immunogenic, and minimize an inflammatory response upon implantation. In some cases, tunable biodegradability is employed and can be important in allowing for deposition of ECM produced by the

proliferating cells in engineered tissue (Gopinathan and Noh, 2018). The abovementioned properties are largely related to the overall biocompatibility of a material and can be fine tuned by adjusting the chemical composition and formulation of a bioink.

1.2.2 Traditional Bioinks

The evolution of tissue engineering from traditional biofabrication techniques and hydrogels for cell culture naturally progressed to using the same traditional hydrogels as bioinks for 3D bioprinting. These hydrogels include an array of both natural and synthetic polymers (Gungor-Ozkerim *et al.*, 2018). Some of the most popular hydrogels used for bioinks are summarized in the tables below:

Table 1-1 Natural polymers traditionally used as bioinks.

Bioink/ Polymer	Background Information	Crosslinking Method	Notable Properties	Ref.
Agarose	Polysaccharide extracted from marine algae and seaweed	Thermal	Biocompatible and non-cytotoxic, no cell binding sites	(Gungor-Ozkerim *et al.*, 2018)
Alginate	Polysaccharide derived from brown algae	Ionic (Ca^{2+}, Mg^{2+}, Ba^{2+})	Biocompatible, low cytotoxicity, fast gelation, ionic crosslinks can be removed	(Gungor-Ozkerim *et al.*, 2018)
Collagen	Main structural protein in the ECM	Physical (pH mediated) and thermal	Highly biomimetic and biocompatible, contains cell binding sites.	(Caliari and Burdick, 2016)
Chitosan	Polysaccharide from deacetylation of chitin	Ionic, pH	Antibacterial, hemostatic, good for wound healing	(Hospodiuk *et al.*, 2017)

Fibrinogen/ Fibrin	Protein important in the blood clotting cascade	Ionic (Ca^{2+}), enzymatic (thrombin)	Low viscosity, fast and irreversible gelation, highly cell adherent	(Hospodiuk *et al.*, 2017)
Gelatin	Denatured collagen	Thermal, enzymatic	Highly biomimetic and biocompatible, contains cell binding sites, gel to solution transition at 25-35℃	(Panwar and Tan, 2016)
Hyaluronic Acid	Glycosamino-glycan (GAG) found in ECM	Physical (pH mediated)	High biocompatibility, form flexible hydrogels, slow gelation rate, poor mechanical strength	(Hospodiuk *et al.*, 2017)

Table 1-2 Synthetic polymers traditionally used as bioinks

Bioink/ Polymer	**Background Information**	**Crosslinking Method**	**Notable Properties**	**Ref.**
Poly-ethylene glycol (PEG)/ PEG diacrylate (PEGDA)	Synthesized by ethylene oxide polymerizatio n and frequently chemically modified	Many types – depending on chemical modification (UV crosslinking with diacrylate group modification)	Highly tunable polymerization, good mechanical strength, non-cytotoxic	(Gungor-Ozkerim *et al.*, 2018)
Pluronic	Tri-block polymer with two hydrophilic blocks and one hydrophobic block	Thermal	Reverse gelation (liquid to gel transition at ~20℃), often used as a sacrificial material	(Hospodiuk *et al.*, 2017)

1.2.3 Advanced Bioinks

As the field of 3D bioprinting has progressed, bioinks have also undergone many developments. The main goal in developing advanced bioinks is to maximize both printability and biocompatibility to ease the fabrication process and allow for clinically relevant 3D structures, all while maintaining high cell viability and the ability of the 3D bioprinted tissue construct to mature into functional tissue (see Figure 1-6) (Chimene *et al.*, 2016).

There are four general strategies in preparing advanced bioinks which involve combining or chemically modifying traditional bioinks with other materials or moieties, respectively in order to optimize the properties. The first strategy, multimaterial bioinks, incorporates multiple compounds into a bioink and crosslinks them together (Chimene *et al.*, 2016). For

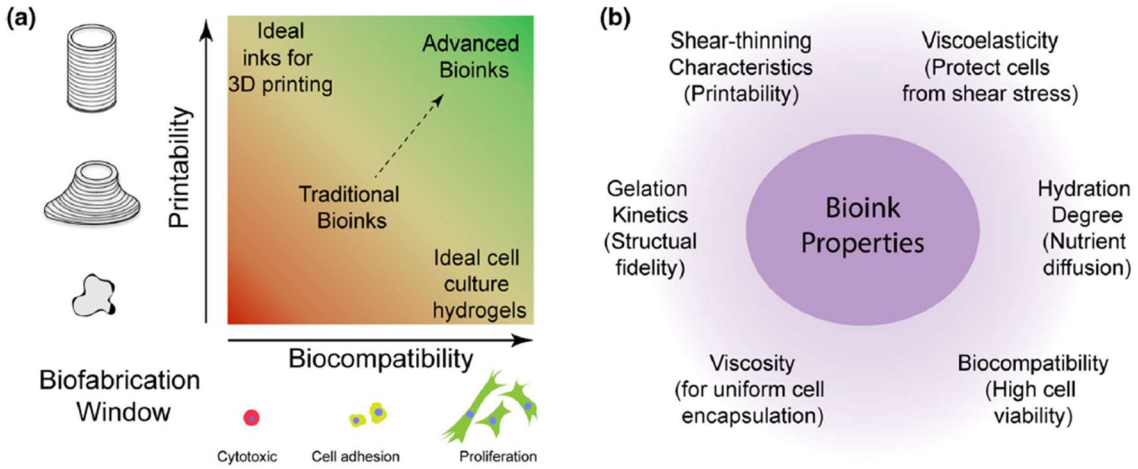

Figure 1-6 A summary of advanced bioink properties (a) The biofabrication window illustrates the desired combination of both printability and biocompatibility in advanced bioinks. (b) The associated properties to be optimized in an advanced bioink. Reprinted with permission from Springer Nature (Chimene *et al.*, 2016).

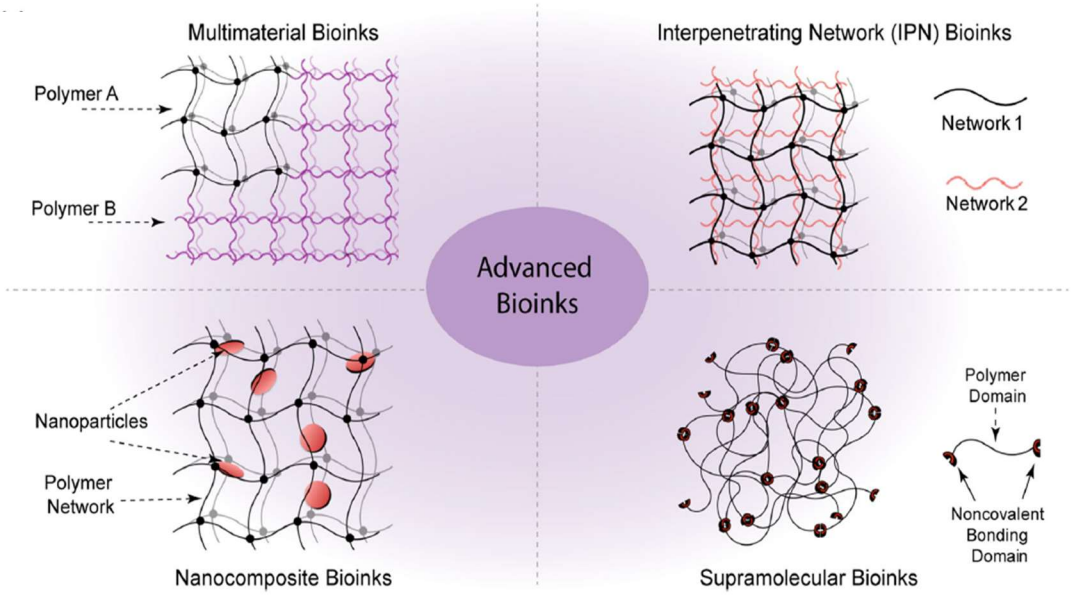

Figure 1-7 Visual representation of the general strategies in preparing advanced bioinks. Reprinted with permission from Springer Nature (Chimene *et al.*, 2016).

example, crosslinking gelatin with PEG was shown to improve mechanical integrity of printed constructs at physiological temperature while maintaining the cell compatibility properties of gelatin (Rutz *et al.*, 2015). The second strategy, interpenetrating networks (IPNs), combines two or more polymers that have limited molecular interactions with one another, resulting in physical entanglement of the polymer chains (Chimene *et al.*, 2016). In some cases, multiple crosslinking methods may be employed and IPNs are known to have enhanced toughness and resistance to fracturing. The third strategy, nanocomposite bioinks, incorporates nanoparticles into a polymer solution for a variety of different functions both related to the mechanical integrity of the bioink and specialized properties such as bioactivity, controlled drug release, electrical conductivity, photo-responsiveness, and magnetism. Both nanosilicates and nanocellulose have been explored for their ability to impose shear thinning behaviour in hydrogels (Avery *et al.*, 2016; Martínez Ávila *et al.*,

2016; Jin *et al.*, 2017; Sultan *et al.*, 2017). The last strategy, supramolecular bioinks, employ the use of different functional units within a polymer to generate non-covalent interactions between entangled polymer chains (Chimene *et al.*, 2016). These non-covalent interactions can be reversibly broken when exposed to physical stresses, improving the shear thinning behaviour of the bioink. The four general strategies in formulating advanced bioinks are represented in Figure 1-7.

1.3 3D Bioprinted Scaffold Design

As previously mentioned, 3D bioprinting offers a great deal of control over the architecture of 3D bioprinted tissues. In the design of hydrogel scaffolds for tissue engineering, certain criteria must be met while optimizing the design of scaffold architecture. For example, the shape and size of the engineered tissue must be equal or complementary to the native tissue, the scaffold architecture should support the diffusion of nutrients, gas, and biomolecules to support cell viability, the scaffold should possess suitable degradation kinetics to allow for tissue growth and infiltration of the surrounding tissue, the scaffold should support spatiotemporal control for multiple cell types, and, lastly, the scaffold must be able to resist stresses found *in vivo* with sufficient strength and toughness (Williams *et al.*, 2018).

Apart from the controllable parameters that go into formulating an effective bioink, the architectural design of a scaffold has powerful influence over the abovementioned criteria. For example, the diffusion of gas, nutrients, and biomolecules can be directly influenced by the porosity of the scaffold and the printed fiber size if cells are encapsulated (Woodfield *et al.*, 2004). Increased porosity and decreased fiber size allow for better mass transport, or

increased permeability, throughout the scaffold and into the hydrogel, respectively. Porosity and fiber size exhibit control over the degradation of scaffolds by influencing scaffold exposure to the surrounding fluid environment (Agrawal *et al.*, 2000; Chen, Zhou and Li, 2011). Furthermore, sufficient porosity and permeability supports better cell seeding within the scaffolds, as well as improved cell and tissue invasion after implantation. Scaffold design can also be employed to exhibit spatiotemporal control over cell types. For example, 3D bioprinting multiple bioinks in the same scaffold structure with or without cells can be used to direct cell growth (Hong *et al.*, 2015; Rutz *et al.*, 2015). A composite scaffold of gelatin and PEG was shown to promote cell growth only on the gelatin fibers of the 3D bioprinted scaffold, which could enable the use of PEG for other functions such as a structural support, degradation moderator, or biomolecule delivery system (Rutz *et al.*, 2015). Another interesting example shows that architectural shape has influence over the growth and maturation of heart tissue (Engelmayr Jr *et al.*, 2008). Honeycomb shaped scaffolds were shown to improve cardiac cell alignment and allow for anisotropic contraction of engineered tissue matching that of an adult rat native myocardial tissue. Lastly, 3D printed scaffold design has great influence over the mechanical strength of an engineered tissue construct (Kelly *et al.*, 2018). Not only the level of porosity, but the printed scaffold pattern has been shown to influence the mechanical strength of a scaffold in several metal, ceramic, and stiff polymer scaffolds for tissue engineering. This effect has been studied for stiffer tissues such as bone due to the inherent higher mechanical strength, allowing for easy characterization of the effect with traditional mechanical characterization methods. Overall, altering the architecture of a scaffold to optimize it for

a desired tissue engineering application will affect the overall mechanical strength of the scaffold, further affecting its ability to withstand stresses experienced after *in vivo* implantation.

1.4 Mechanical Characterization of 3D Bioprinted Constructs

The mechanical properties of 3D bioprinted constructs are subject to detailed investigation as part of the *in vitro* characterization to determine viability of an engineered tissue. Methods of measuring bulk soft hydrogel materials can be similar to traditional structural analysis in that we can compress, bend, twist, and stretch them to monitor their mechanical properties, all of which destroy the sample (*Instron Biomaterials - Instron*, 2019). However, low force conditions and high resolution sensitivity are often necessary since these materials are soft in nature. Another interesting characteristic of these materials that makes it challenging to measure their physical properties is that they exhibit a high level of viscoelasticity. Viscoelastic materials exhibit both viscous and elastic characteristics under stress and deformation (Yousefzadeh, 2017). For example, a viscous material will exhibit time dependent behaviour while under stress and does not have any "memory" of its original configuration (Papanicolaou and Zaoutsos, 2011). Whereas an elastic material exhibits instantaneous deformation under stress and will return to its original state when the stress is removed. A viscoelastic material exhibits both of these characteristics with time-dependent strain and a "fading memory." This, consequently, gives hydrogels the ability to exhibit flow-like properties, and, thus, rheological measurements can also be used to determine the mechanical properties of hydrogels.

Viscoelasticity can be quantified in a few different forms. The storage modulus, or G', is a measure of the elastic component of a viscoelastic material (Barsoum, 2015). It is related to the energy stored in the material during deformation. The loss modulus, or G", is a measure of the viscous component of a viscoelastic material. It is related to the energy dissipated or lost from the material during deformation. These two terms can be used to calculate the complex modulus, or G*, via the following formula:

$$G^* = G' + iG" \tag{1-1}$$

where i is the imaginary number, $\sqrt{-1}$. The complex modulus is can be expressed as an absolute value that takes into consideration the overall viscoelasticity of a material. G' and G" can also be used to calculate the loss factor, or tanδ, via the following equation:

$$tan\delta = \frac{G"}{G'} \tag{1-2}$$

where δ is the phase angle between the storage and loss modulus. A loss factor below 1 indicates more solid like behaviour.

Accurate characterization of the mechanical properties of implantable materials can be the difference in determining the success of an implant. For example, in the case of engineering regenerative tissue to repair myocardial infarction (scarred heart after a heart attack), matching the mechanical properties of the native tissue is of utmost importance (Jackman *et al.*, 2018). A large mismatch in mechanical properties between the native tissue and the implanted tissue has the potential to cause an inflammatory response, which can be fatal for some patients.

A recent comprehensive review on the effect of scaffold design on function exemplified compression testing as the most widely used method of measuring the mechanical strength

of 3D printed scaffolds for tissue engineering (Kelly *et al.*, 2018). Other traditional methods of analysis often used in characterization of a bulk hydrogel material, such as rheometry, atomic force microscopy, and particle tracing microrheology are effective in measuring the bulk material and microstructural mechanical properties of bioinks, but are incompatible with measuring the effect of 3D bioprinted architecture on the scaffold mechanical strength (Kloxin *et al.*, 2010). Interestingly, the range of 3D bioprinted scaffold architectural analyses in the literature does not reach a stiffness below the MPa scale (Kelly *et al.*, 2018). Soft tissues, which are often engineered with hydrogel scaffolds, are on the order of Pa and kPa stiffness (Discher, Mooney and Zandstra, 2009). This deficit in the literature of characterizing the effect of 3D bioprinted architecture suggests the ineffectiveness of compression testing in measuring the soft stiffnesses of 3D bioprinted hydrogel scaffolds widely used in tissue engineering. This is likely due to the delicate and often imperfect structure of 3D bioprinted hydrogel scaffolds. Furthermore, the aforementioned recent review on 3D bioprinted architecture's effect on mechanical and functional properties noted a deficit in the literature investigating this effect and corroborated it with another review by Zadpoor *et al.* (Zadpoor, 2017; Kelly *et al.*, 2018).

1.5 Conclusion

3D Bioprinting is an emerging field that has great potential to address many of the challenges in the field of tissue engineering. This has led to significant investment in developing effective 3D bioprinting platforms including inkjet bioprinting, microextrusion bioprinting, laser assisted bioprinting, and stereolithographic bioprinting. Each of these methods has their own individual advantages, however, microextrusion bioprinting is most

commonly employed due to its affordability and versatility in generating clinically relevant engineered tissue. Furthermore, the development of novel bioinks has advanced the field further. The goal of improving both biocompatibility and printability in bioinks has generated an active research field of advanced bioinks.

The parameters involved in the 3D bioprinting process allow for a high level of optimization of scaffolds for engineered tissue. The selection of 3D bioprinting technique, formulation of the bioink, and design of the 3D bioprinted scaffold architecture employ a great deal of influence on the final engineered tissue construct. Currently, *in vitro* characterization of the mechanical and physical properties of 3D bioprinted hydrogel scaffolds often relies on the characterization of the bulk bioink material and not the 3D printed construct. This characterization of the bioink mechanical properties is very important for determining cytocompatibility but ignores the important consideration of mechanical durability in an *in vivo* implantation site. This effect of 3D printed architecture on mechanical and functional tissue properties has been studied in the area of bone tissue engineering where the scaffolds are stiff enough for effective characterization using compression testing, however, there is a discrepancy in the literature for relationships between structure and function of 3D bioprinted architectures in soft hydrogel scaffolds. This demonstrates a great need for a new method of characterizing the effect 3D bioprinted architecture on the mechanical and physical properties of 3D bioprinted hydrogel scaffolds. The remainder of this thesis will focus on the development of a novel characterization method to develop relationships between structure and function of 3D bioprinted hydrogel scaffolds.

Chapter 2 Development of a Novel Characterization Method of 3D Bioprinted Hydrogel Scaffolds

Rheolution, a Canadian company based out of Montreal, has invented a new technology that has proven to be effective in monitoring the viscoelastic properties of hydrogel materials (*Rheolution Inc. - Soft Materials Testing Instruments*, 2019). Their technique, viscoelastic testing of bilayered materials (VeTBiM), non-destructively characterizes the viscoelastic properties of hydrogels (Ceccaldi *et al.*, 2017). A non-destructive and contactless measurement introduces practicality into time-dependent studies of the mechanical properties of hydrogels and lends itself as a platform for monitoring the bulk mechanical properties of 3D bioprinted hydrogel scaffolds. Their instrument, the ElastoSens Bio^2 has the ability to measure viscoelastic properties, namely the storage modulus and the loss modulus, which relate to the elastic and viscous properties of the hydrogel, respectively. Using the G' and G", The complex modulus, G*, and the loss factor, tanδ, can also be calculated. The instrument conducts the measurement by applying

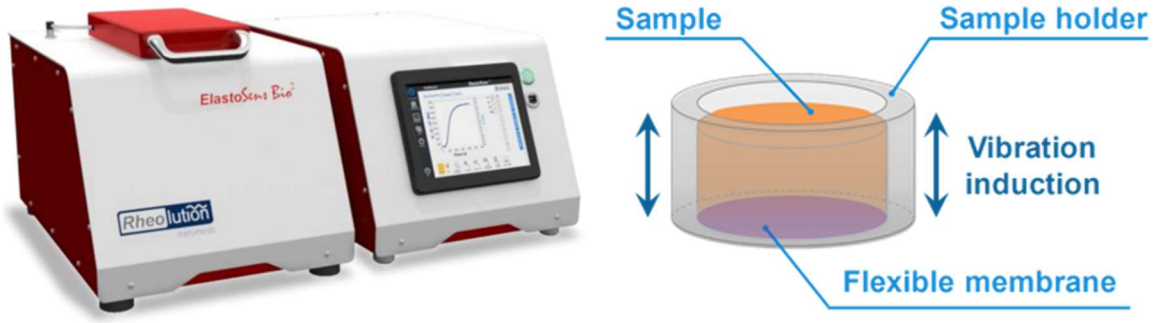

Figure 2-1 The ElastoSens Bio^2 measures the viscoelastic properties of hydrogels by applying a vibration to the sample in a specialized sample cup (*Rheolution Inc. - Soft Materials Testing Instruments*, 2019).

a low-amplitude vibration to the sample and monitoring its displacement with an ultrasonic and laser sensor during the material's first three eigenfrequencies. In order to do this, the sample is loaded into a cylindrical sample cup which has grooves on its walls and a silicone membrane for the bottom of the cup (see Figure 2-1). This allows for a liquid-tight seal around the bottom and holds the sample completely still at the walls of the cup, while allowing for vibration in the Z-axis.

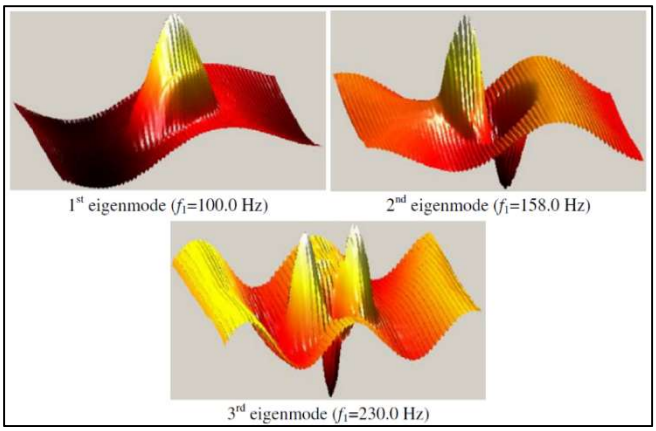

Figure 2-2 The first three eigenmodes of a plate structure. Reproduced from with permission from Elsevier (Henni, Schmitt and Cloutier, 2010).

The theory behind calculating the viscoelastic properties of the sample lies behind the idea that the sample is acting as a bilayered plate with predicted eigenmodal behaviour (Henni, Schmitt and Cloutier, 2010). In consideration of the plate like behaviour, the material can then be expected to have the first three eigenmodes as shown in Figure 2-2**.** A further consideration of the system can be defined with the following equation that applies to the bending of a plate:

$$\boldsymbol{D = \frac{E h_e^3}{12(1 - v^2)}} \tag{2-1}$$

where D is the flexural rigidity of the plate, E is the Young's modulus, h_e is the thickness of the plate, and v is the Poisson's ratio of the material. Using Rheolution's proprietary model as a standard curve with the measured eigenfrequencies, the instrument is able to convert the analyzed measurement to the shear storage and loss modulus of the sample (Henni and Schmitt, 2019).The adjustable parameters of the instrument only pertain to the environmental conditions, such as temperature, and the time of measurement. Adjustments of the sample vibration conditions are not possible with this instrument. Furthermore, vibration is only possible in the vertical direction, determining the uniaxial measurement of the viscoelastic properties. Assumptions that the instrument makes include the following:

- There is no movement of the sample at the walls of the sample cup
- The sample is in contact with the silicone membrane on the bottom of the cup
- The sample is in the shape of a disk
- The sample has a density of 1g/ml (which is the case for hydrogels)

Considering the theory behind how the instrument works and the assumptions that are made, the instrument seems fit for analyzing the overall mechanical properties of 3D bioprinted scaffolds with varying architectural designs provided that the sample in the cup meets all the abovementioned assumptions. The following chapter outlines the development of a novel characterization method using the ElastoSens Bio^2 for characterizing the viscoelastic properties of 3D bioprinted hydrogel scaffolds for applications in tissue engineering. First, a strategy for characterization of 3D bioprinted scaffolds will be proposed, followed by selection of the bioprinting technique and bioinks

to be used for the development of the method, and, finally, an assessment of the 3D bioprinting conditions for generating scaffolds.

2.1 Materials and Methods

2.1.1 Proposal of Sample Preparation for Analysis of 3D Bioprinted Scaffolds

In order to for an accurate measurement of the viscoelastic properties of 3D bioprinted scaffolds, all the assumptions that the ElastoSens makes in its measurement must remain correct. Bioinks must be printed inside of the sample cup to adhere the scaffold to the elastic membrane with a border printed around the edge of the scaffold to fix the scaffold

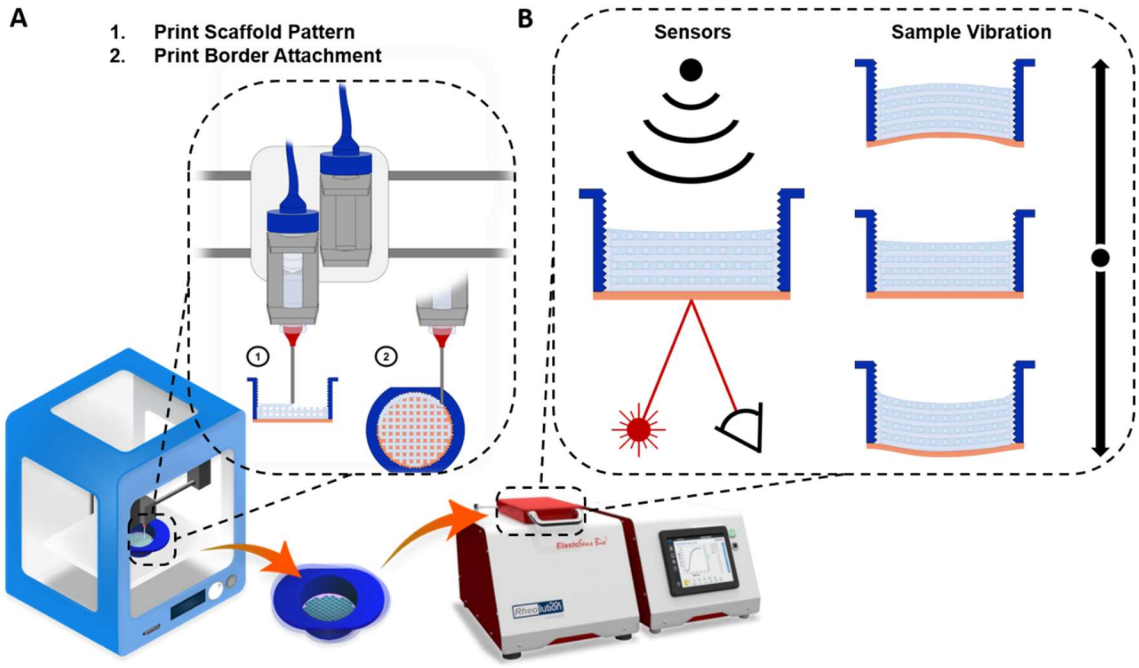

Figure 2-3 Proposed method of sample preparation for measurement of viscoelastic properties of 3D bioprinted scaffolds. (A) Microextrusion bioprinting is employed to print a scaffold in the sample cup with a border around the scaffold to attach the sample to the walls of the sample cup. (B) The scaffold is filled in with aqueous solution and analyzed with the ElastoSens Bio^2.

against the grooved walls of the sample cup (see Figure 2-3). In order to print inside of the cup and form high fidelity printed scaffolds, microextrusion bioprinting was chosen for its ability to use a long needle for printing inside the cup and its ability to print bioinks with higher viscosity. The use of microextrusion bioprinting also allows for over-extrusion of material to push bioink into the wall grooves of the sample cup, attaching the scaffold to the wall. Once the scaffold is printed in the sample cup, filling it in with water accounts for the assumption that the density of the sample is ~1g/ml and the entire structure, including the scaffold and filling solution, is in the shape of a disk.

2.1.2 Selection and Preparation of Bioinks

Alginic acid sodium salt (Alginate), poly-ethylene glycol diacrylate (PEGDA), gelatin from porcine skin (type A, 300 bloom gel strength), calcium chloride, and 2-Hydroxy-4′-(2-hydroxyethoxy)-2-methylpropiophenone (photo-initiator) were all acquired from Sigma Aldrich, St. Louis, Missouri. Laponite XLG, a synthetic nanosilicate, was acquired from BYK additives, Germany. For consistent print fidelity and the ability to print free standing scaffolds before crosslinking, nanocomposite bioinks using Laponite as an internal scaffold were chosen and adapted from two previous methods (Avery *et al.*, 2016; Jin *et al.*, 2017). For the purposes of this thesis, all following concentrations of solutions are (w/v%). 0.5% Alginate, 6% Laponite (Alg/Lap) was prepared by, first, dissolving alginate in deionized water and cooling the solution to 4°C. Laponite was added to the solution and immediately vortexed for 2-4 minutes to ensure homogenous distribution of laponite in solution. Laponite takes time for water molecules to adsorb to the surface of nanoparticles, delaying the formation of a more viscous gel. While the laponite was not fully hydrated and the

mixture exhibited a low viscosity, the solution was degassed in a vacuum chamber. 2.5%, 5%, and 10% PEGDA, 6% Laponite, and 1% photo-initiator (PEGDA/Lap) was prepared by, first, dissolving photo-initiator in deionized water, adding the necessary volume of PEGDA, and cooling the solution to 4℃. Laponite was added to the solution and immediately vortexed for 2-4 minutes to ensure homogenous distribution of laponite in solution. While the laponite was not fully hydrated, the solution was degassed in a vacuum chamber. Where the concentration of PEGDA is not explicitly labeled, the 5% PEGDA/Lap formulation is used. 5.6% gelatin, 3.4% Laponite (Gel/Lap) was prepared by, first, preparing a solution of 18% gelatin in de-ionized water at 50℃. A solution of 9% Laponite was prepared by adding Laponite to 4℃ deionized water and immediately vortexing until a stable, homogenous gel formed. The 9% Laponite solution was heated to 50℃. The gelatin solution was diluted by half with 50℃ deionized water without mixing, and enough 9% Laponite was added to dilute to the final concentrations of 5.6% gelatin, 3.4% Laponite. The mixture was immediately vortexed until a homogenous, viscous gel formed. The gel was reheated to 50℃ and degassed in a vacuum chamber. All gels were stored in the refrigerator and allowed to hydrate overnight before 3D bioprinting. PEGDA/Lap was protected from light to prevent unwanted crosslinking. 2% calcium chloride in deionized water was prepared to crosslink Alg/Lap post bioprinting. 365nm UV light was used to crosslink PEGDA/Lap post bioprinting.

2.1.3 3D Bioprinting Assessment of Bioinks

All 3D bioprinting experiments for this thesis were conducted using a Cellink Inkredible+ (Cellink, Sweden) microextrusion 3D bioprinter with pneumatic pressure to

extrude materials. Repetier software was used to manually prepare codes for the printing assessment of each bioink. Both printhead speed and different needle gauges were used to alter the diameter of printed fibers and determine a working size range of printable fibers. The printing air pressure was determined for each individual bioink and optimized to match the printing speed so that circular fibers would be deposited in the scaffold architectures. Gel/Lap was printed with a heated aluminum print cartridge (Cellink) at 50°C. Printed fiber cross-sections were imaged on a Zeiss Axio Observer 5 microscope (Zeiss, Germany) and the cross-section circularity of fibers was determined by the following formula:

$$Circularity = \frac{4\pi Area}{Perimeter^2} \quad (2\text{-}2)$$

The cross-section circularity was used as a measure of print fidelity to show the retention of circular shape after being deposited on the substrate.

2.1.4 Comparison of Rheometer and ElastoSens Measurements with Bulk Bioinks

Measurements of the bulk bioinks were conducted with both a rheometer and the ElastoSens to validate the accuracy of the ElastoSens measurements. All experiments were conducted at 37°C. The rheometer measurements were conducted with 1Hz frequency and 0.5% strain. The storage and loss moduli were measured with both methods for comparison.

2.1.5 Statistical Analysis

All experiments were conducted in triplicate and the data were expressed as the mean ± standard deviation. Statistical analysis was conducted using two-way ANOVA on the

appropriate experimental groups. *P* values < 0.05 were deemed as statistically different and *p* values < 0.01 were deemed extremely significant.

2.2 Results and Discussion

The proposal of a 3D bioprinted scaffold sample preparation method for analysis with the ElastoSens Bio^2 was included in this section to justify the choices of 3D bioprinting technique and bioinks. Microextrusion bioprinting was the best fit for 3D bioprinting in the ElastoSens Bio^2 sample cups for its versatility and compatibility with high viscosity bioinks (Pedde *et al.*, 2017). Achieving high print fidelity is an important bioink property to ensure consistency in production of 3D bioprinted samples. With lower viscosity bioinks, the risk of sample spreading and the inability to fabricate multi-layered constructs with consistent layer height would impose unnecessary difficulty for a proof of concept.

Three traditional hydrogels were chosen to as a representative set of materials commonly used within the field of 3D bioprinting. Alginate, a polysaccharide derived from brown algae, can be chemically crosslinked at a fast rate with calcium ions and exhibits high biocompatibility (Gungor-Ozkerim *et al.*, 2018). PEGDA, a synthetic polymer that is UV crosslinkable in the presence of a photo-initiator, is a popular choice for 3D bioprinting due to its good mechanical strength, low cytotoxicity, and tunable polymerization. Lastly, gelatin is a denatured form of collagen, a common ECM protein (Panwar and Tan, 2016). It exhibits high biocompatibility, peptide sequences which allow for cell binding, and is thermally and enzymatically crosslinkable.

The use of nanocomposite bioinks with Laponite, a synthetic nano-silicate with a platelet structure and charged surfaces, allows for improved shear thinning behaviour as

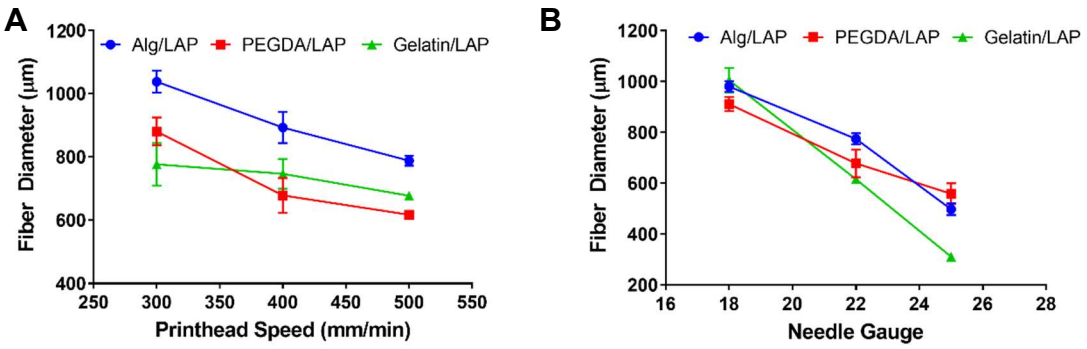

Figure 2-4 Both printhead speed (A) and needle gauge (B) are capable of controlling the printed fiber diameter.

exemplified in many other studies (Gaharwar *et al.*, 2014; Au *et al.*, 2015; Avery *et al.*, 2016; Chimene *et al.*, 2016; Jin *et al.*, 2017; Peak *et al.*, 2018). This shear-thinning behaviour is induced by weak electrostatic interactions that can be reversibly broken when shear stress is applied, thus reducing the viscosity of the bioink. Shear-thinning is important in both the formation of consistent free-standing scaffold structures that do not require crosslinking during the printing process and for the ability to overextrude the bioink into the grooved sample cup walls for successful attachment of the scaffold to the sample cup. The bioink preparation process included a degassing step to prevent the 3D bioprinted scaffolds from floating in the sample cup and promoting adherence to the elastic membrane. As previously mentioned, both the printhead speed and needle gauge were useful tools in tuning the size of printed fibers. All three bioinks exhibited fiber diameters that were dependent on the speed that the printhead was moving (see Figure 2-4). A smaller fiber size was associated with a faster printhead speed showing that the fibers either overextrude at slower speeds or become stretched at higher print speed. Furthermore, the choice of needle gauge exhibited further control over fiber diameter with a wider range of

printed fiber sizes and less variability in fiber diameter between samples. The fiber diameter ranges of all three bioinks were in the range of ~400 or ~500 µm in diameter up to ~1mm. This range in fiber diameter is sufficient for future studies in varying the printed fiber size.

The cross-section circularity of each bioink was assessed to exemplify print fidelity in 3D printed fibers and scaffolds (see Figure 2-5). All three bioinks exhibit high print fidelity

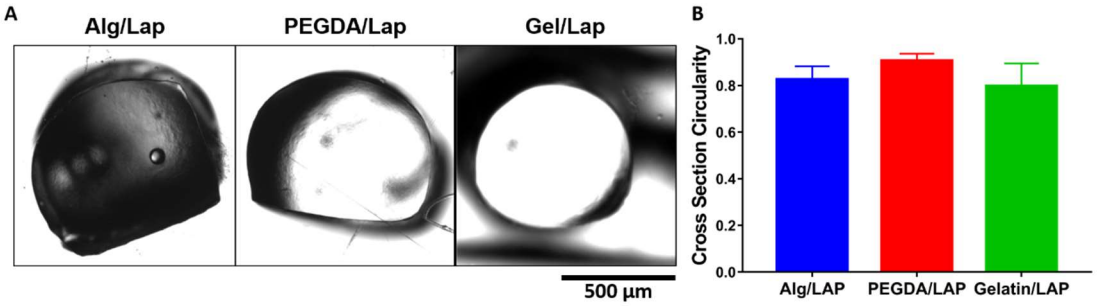

Figure 2-5 (A) Cross-section circularity images and (B) quantification exemplifies high print fidelity for all three bioinks.

with cross section circularities above 0.8 (1.0 being a perfect circle). This will enable the printing of consistent hydrogel scaffold for further experiments.

A rheometer was used to compare the accuracy of the ElastoSens measurements for the bulk materials used in this thesis. Both Alg/Lap and PEGDA/Lap show the similar storage

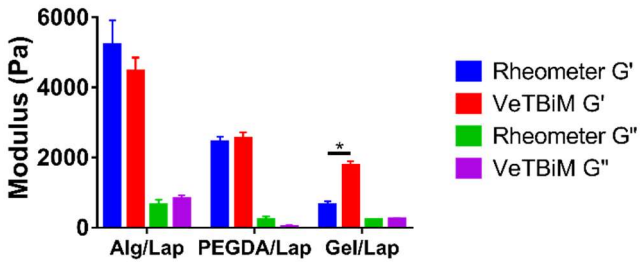

Figure 2-6 Comparison of viscoelastic properties measured by rheometer and VeTBiM shows that Alg/Lap and PEGDA/Lap are suitable materials for this method of characterization.

and loss moduli measured by each method, however, Gel/Lap was shown to have a higher storage modulus measured with VeTBiM. This is likely due to the material exhibiting stiffness approaching the detection limit of the instrument. For the remainder of the thesis, Alg/Lap and PEGDA/Lap will be used to conduct proof of concept experiments to demonstrate the potential usefulness of the developed method.

2.3 Conclusion

Rheolution's VeTBiM technology presents itself as a potential platform for analyzing the effect of 3D bioprinted architecture on scaffolds for tissue engineering. A method for using the ElastoSens Bio^2 was proposed by using microextrusion bioprinting to print scaffolds directly in the instrument's specialized sample cups, fixing the sample within the cup and filling the sample in with aqueous solution. This method fulfils the required assumptions of the instrument deemed necessary in providing an accurate measurement of viscoelastic properties. Nanocomposite bioinks, Alg/Lap, PEGDA/Lap, and Gel/Lap, were chosen for their high print fidelity and shear thinning capability. These beneficial properties will enable easy fabrication of consistent scaffolds within the sample cups. The ability to alter the printed fiber size by changing the printhead speed or needle used will enable characterization of varying scaffold designs and overextrusion of bioink into the grooved walls of the sample cups for effective attachment of the sample to the cup. Both Alg/Lap and PEGDA/Lap bulk mechanical properties were measured accurately with VeTBiM as confirmed by using a rheometer. The choice in bioprinting method, bioink, and development of an effective protocol for sample preparation will be useful tools in a proof-

of-concept study to demonstrate the ElastoSens Bio^2's potential ability of characterizing 3D bioprinted scaffolds.

Chapter 3 Proof-of-Concept Studies in Characterizing the Effect of 3D Bioprinted Scaffold Architecture on Function

As discussed in previous chapters, engineered tissue products suffer from a pre-clinical bottleneck which prevents translation from the research lab to clinical trials, and further on to commercialization. The inability to fabricate tissues with comparable complexity to native tissues in the body imposes this bottleneck within the field (Atala, Kurtis Kasper and Mikos, 2012). However, 3D bioprinting is touted as a promising solution that can address the shortcomings of traditional biofabrication methods with unparalleled ability to spatially arrange cells, biomaterials, and biomolecules with complex architecture that mimics native tissue (Murphy and Atala, 2014). The parameters involved in 3D bioprinting, including 3D bioprinting technique, bioink composition and formulation, and 3D bioprinted scaffold architecture, offer a great deal of control over generating tissue for any desired tissue type. Furthermore, recent reviews which study the effect of 3D printed architecture on the mechanical properties and functionality of 3D printed scaffolds point out a deficit in the literature for understanding relationships between structure and function of scaffolds, as well as no existence of literature which characterizes the effect of scaffold design for soft tissue scaffolds in the range of Pa-kPa (Discher, Mooney and Zandstra, 2009; Zadpoor, 2017; Kelly *et al.*, 2018). Another recent review on advancing the field of 3D bioprinting by Jakus *et al.* calls for new methods of characterizing 3D bioprinted scaffolds, considering it a critical necessity for advancing the field (Jakus, Rutz and Shah, 2016).

In this thesis, a new method of characterizing 3D bioprinted scaffolds for tissue engineering has been developed using VeTBiM technology developed in Canada (*Rheolution Inc. - Soft Materials Testing Instruments*, 2019). Rheolution's instrument, the ElastoSens Bio^2, uses contactless and non-destructive vibrational induction paired with a laser and ultrasound sensor to monitor the vibrational response of hydrogels (Ceccaldi *et al.*, 2017). This response can then be used with their proprietary model to determine the viscoelastic (G' and G") properties of the hydrogel sample. The innovation in this project comes from the novel idea to employ this technology as a method for analyzing 3D bioprinted scaffolds and in the effective sample preparation which fulfils the requirements necessary to deem a measurement as accurate. Furthermore, non-destructive and contactless mechanical properties characterization allows for time-dependent studies without the need for rigorous and expensive sample preparation. To date, no such characterization has been published in the literature for soft materials in the Pa-kPa range used for soft tissue engineering.

In order to effectively characterize 3D bioprinted hydrogel scaffolds with consistent shape and structure, alginate, PEGDA, and gelatin supplemented with Laponite to improve printability and shear thinning behaviour were used as bioinks. Each of the bioinks have different crosslinking mechanisms: Alg/Lap is crosslinked ionically by Ca^{2+}, PEGDA/Lap is crosslinked with UV light, and Gel/Lap is crosslinked thermally. Alginate, a polysaccharide extracted from brown algae, is effective in 3D bioprinting due to its fast and reversible ionic crosslinking mechanism (Gungor-Ozkerim *et al.*, 2018). PEGDA is a chemically modified version of PEG, one of the most common synthetic polymers that is

known for its tunable polymerization and customizability in forming branched polymers. PEGDA is modified with acrylate groups which are crosslinkable in the presence of a photo-initiator and UV light. Gelatin is denatured collagen, a main component of ECM, and is known for its high biocompatibility and amino acid sequences which allow for cell binding to the polymer. Laponite, a commonly used synthetic nano-silicate, is gaining popularity as an additive for advanced bioinks and has been shown as an effective platform for protein adhesion which further allows cells to bind to the material (Chimene *et al.*, 2016). All three of these hydrogels are commonly used in tissue engineering applications and are suitable candidates to demonstrate the use of this method for mechanical properties analysis of 3D bioprinted scaffolds.

In this proof-of-concept work, a series of 3D bioprinted scaffolds with altered parameters involving the bioink formulation and scaffold design were analyzed with the method proposed in chapter two. Briefly, the architectural design was altered by changing printed fiber size and spacing, altering the infill density (porosity), and altering the printed pattern. The effect of bioink formulation on mechanical properties of 3D bioprinted scaffolds was studied. Finally, a study on the effect of multi-material composite scaffolds was employed, and time-dependent studies on both crosslinking and swelling were employed to further exemplify the versatility of the characterization method and the customizability of 3D bioprinting, respectfully.

3.1 Materials and Methods

3.1.1 3D bioprinted scaffold preparation in ElastoSens Bio^2 sample cups

A Cellink Inkredible+ microextrusion bioprinter (Cellink, Sweden) was employed for all the experiments in this chapter. In order to print inside of the ElastoSens Bio^2 sample cups, 1" long stainless-steel dispensing needles (Amazon) were used. For consistent calibration and centering the 3D bioprinter needle in the sample cup, a fixture was designed in SolidWorks software (Dassault Systems, France) to hold the sample cup in place while printing. The fixture 3D model file was sliced into G-code and 3D printed using Ultimaker Cura software and an Ultimaker 2 3D printer, respectively (Ultimaker, Netherlands) (see Figure 3-1). The fixture was made of poly-lactic acid (PLA). Once the sample cup was fixed on the Inkredible+ sample stage, the printing needle's coordinate system was calibrated to be centered in the middle of the sample cup with the elastic membrane surface as the Z=0 coordinate. After calibration, the sample was printed in the sample cup, printing took anywhere from 5-15 minutes depending on the sample being printed. For each layer,

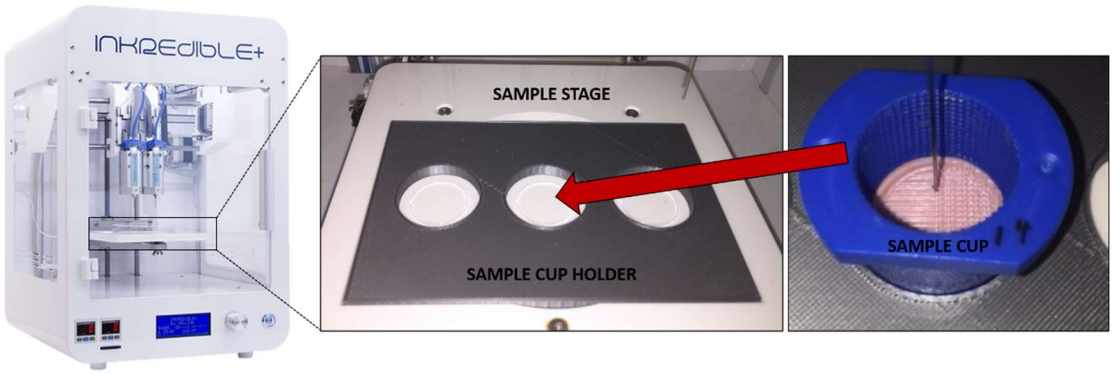

Figure 3-1 A sample cup holder was 3D printed and fixed on the Cellink Inkredible+ stage for consistent calibration and bioprinting of scaffolds.

the scaffold pattern was printed followed by the border attachment. Scaffolds were either filled in with crosslinking solution or with deionized water after crosslinking. All 3D bioprinted scaffold dimensions were a 22mm diameter circular cylinder with 5mm height. All measurements in the ElastoSens Bio^2 were conducted at physiological temperature of 37°C in triplicate.

3.1.2 Effect of fiber diameter and spacing on viscoelastic properties in a rectilinear scaffold

In order to assess the effect of printed fiber diameter and fiber spacing in a traditional rectilinear scaffold, Alg/Lap and 2% $CaCl_2$ were prepared as previously described in chapter 2. Rectilinear scaffold designs were prepared with three different spacings between printed fibers: 1, 1.5, and 2mm (see Figure 3-2). The G-codes for bioprinting these scaffolds were manually prepared using open source Repetier software so that spacing

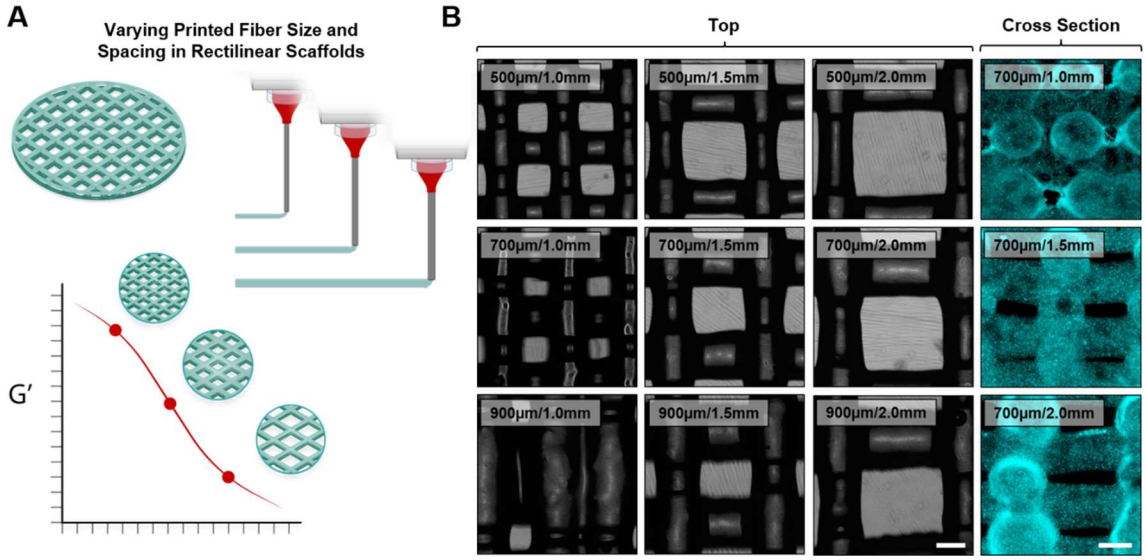

Figure 3-2 (A) Schematic displaying the experimental design – changing the fiber size and spacing influences scaffold strength. (B) Alg/Lap scaffolds with varying spacing and fiber size imaged from above (bright field) and from the cross section (turquoise) (Scale bar = 500µm).

could be customized. Three different needle gauges, 18, 22, and 25, with inner diameters of 0.84, 0.41, and 0.26mm, respectively, were used to generate fiber sizes of ~500, ~700, and ~900 μm. Scaffolds were filled in with 2% $CaCl_2$ and allowed to crosslink for 2 hours at room temperature. Scaffolds were imaged on an Axio Observer 5 microscope (Zeiss, Germany). The bioink was mixed with fluorescent microparticles for imaging the cross sections of the scaffolds. Bulk material samples were prepared by using a syringe to fill the sample cups up to a 5mm sample height.

3.1.3 Effect of 3D bioprinting and fiber diameter on ionic crosslinking time of 3D bioprinting rectilinear scaffolds

In order to assess the effect of fiber diameter on crosslinking time of 3D bioprinted rectilinear scaffolds, Alg/Lap was prepared as described in chapter 2. 3D bioprinted scaffold with ~500 and ~900 μm fiber size scaffolds with 1.5mm spacing were prepared in sample cups as previously stated, and bulk samples were prepared by using a syringe to fill the sample cup up to 5mm height. For the 3D bioprinted scaffolds, 2% $CaCl_2$ was used to fill in the scaffolds and the samples were immediately placed in the ElastoSens Bio^2 for real-time assessment of crosslinking over 2 hours. As a control, deionized water was used to fill in the scaffolds. Three drops of silicone oil (Sigma Aldrich, St. Louis, Missouri) were added to the top of the scaffolds to prevent evaporation of the crosslinking solution during the experiment. For the bulk samples, crosslinking solution or deionized water was added on top of the bioink sheets and removed for measurement at 0, 1, and 2 hours. The measured G' of samples was normalized to the initial value before crosslinking for simple comparison on the same graph. To exemplify the effect of diffusion of Ca^{2+} ions into the

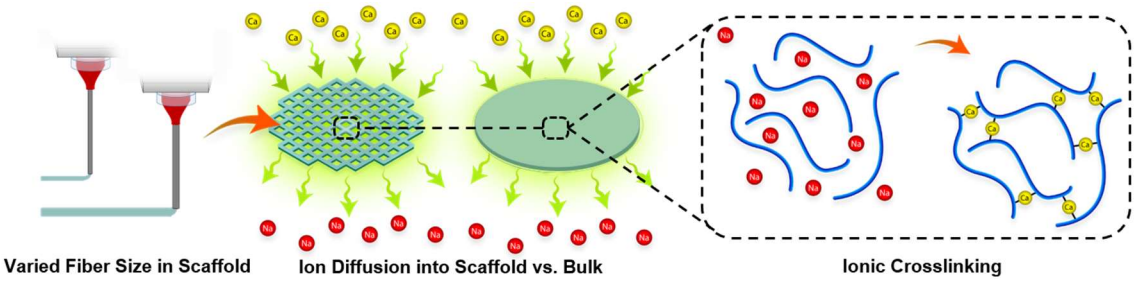

Figure 3-3 Schematic explaining the experimental design – changing fiber size influences ion diffusion and the crosslinking time.

bulk material and 3D bioprinted scaffolds, samples were prepared and immersed in a fluorescent solution of 10 µg/ml a rhodamine B (Sigma Aldrich, St. Louis, Missouri). Diffusion into the scaffolds and bulk material was imaged over 2 hours on a fluorescent microscope and the fluorescence intensity of cross-sections of each sample were plotted against time.

3.1.4 Effect of scaffold infill density on viscoelastic properties of a honeycomb scaffold

In order to determine the effect of infill density, or, in other words, the macro-porosity, of 3D bioprinted scaffolds, PEGDA/Lap was prepared and 3D bioprinted in a honeycomb pattern scaffold. The scaffold designs were prepared by, first, preparing a 3D model of a

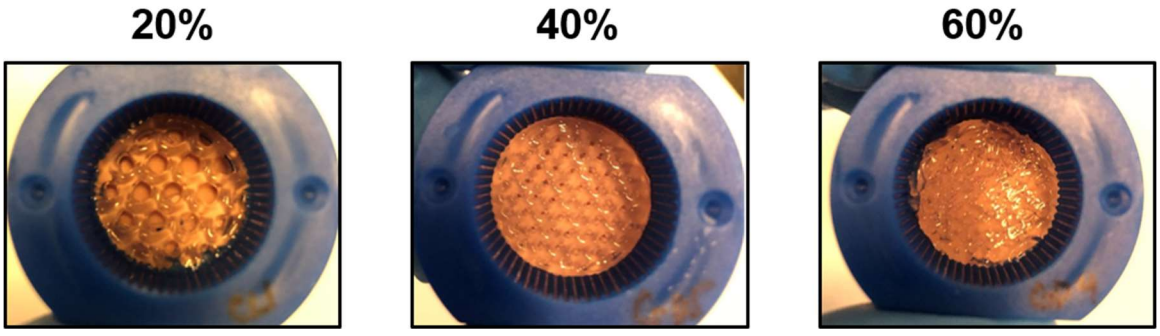

Figure 3-4 Increasing infill density of PEGDA/Lap scaffolds with a honeycomb pattern.

22mm diameter, 5mm high disk using SolidWorks, slicing the file into G-code with open source Slic3r software, and post-processing the G-code with Cellink Heartware software (Cellink, Sweden). Slic3r software has infill designs with adjustable infill density that can be selected for a scaffold pattern. All samples were prepared with a 22G needle and ~700 μm fiber diameter. Infill densities were set at 20, 40, and 60% and samples were crosslinked under UV light for 5 minutes before measurement in the ElastoSens Bio^2 (see Figure 3-4).

3.1.5 Effect of scaffold infill density on swelling rate of a honeycomb scaffold

To further exemplify the effect of infill density on fluid interactions with the surrounding media, PEGDA/Lap honeycomb scaffolds were prepared at 20, 40, and 60% infill density as previously described. Bulk PEGDA/Lap was also prepared in a 5mm thick sheet. Samples were sectioned into smaller pieces and freeze-dried. To assess the swelling rate of samples, samples were weighed at their dry weight and then immersed in 0.1M phosphate buffered saline (Sigma Aldrich, St. Louis, Missouri). Samples were weighed swollen at predetermined time points over 2 hours. Then a final swelling percent was measured at 6 hours. The swelling was calculated using the following formula:

$$Swelling\ \% = \left(\frac{Weight\ (swollen)}{Weight\ (dry)}\right) \times 100\% \tag{3-1}$$

3.1.6 Effect of bioink formulation on viscoelastic properties of 3D bioprinted honeycomb scaffolds

The effect of bioink formulation on the viscoelastic properties of honeycomb scaffold was determined by using three different formulations of PEGDA/Lap bioink. 2.5, 5, and

10% PEGDA/Lap were printed in a 40% infill density scaffold and crosslinked for 5 minutes under UV. Samples were filled in with deionized water and analyzed in the ElastoSens Bio^2.

3.1.7 Effect of printing pattern on the viscoelastic properties of 3D bioprinted scaffolds

To determine the effect of 3D bioprinting pattern on the viscoelastic properties of 3D bioprinted scaffolds, PEGDA/Lap scaffolds were bioprinted three different patterns while keeping the infill density and bioink formulation constant at 20% and 5% PEGDA/Lap, respectively. The patterns, rectilinear, honeycomb, and random line, were selected from

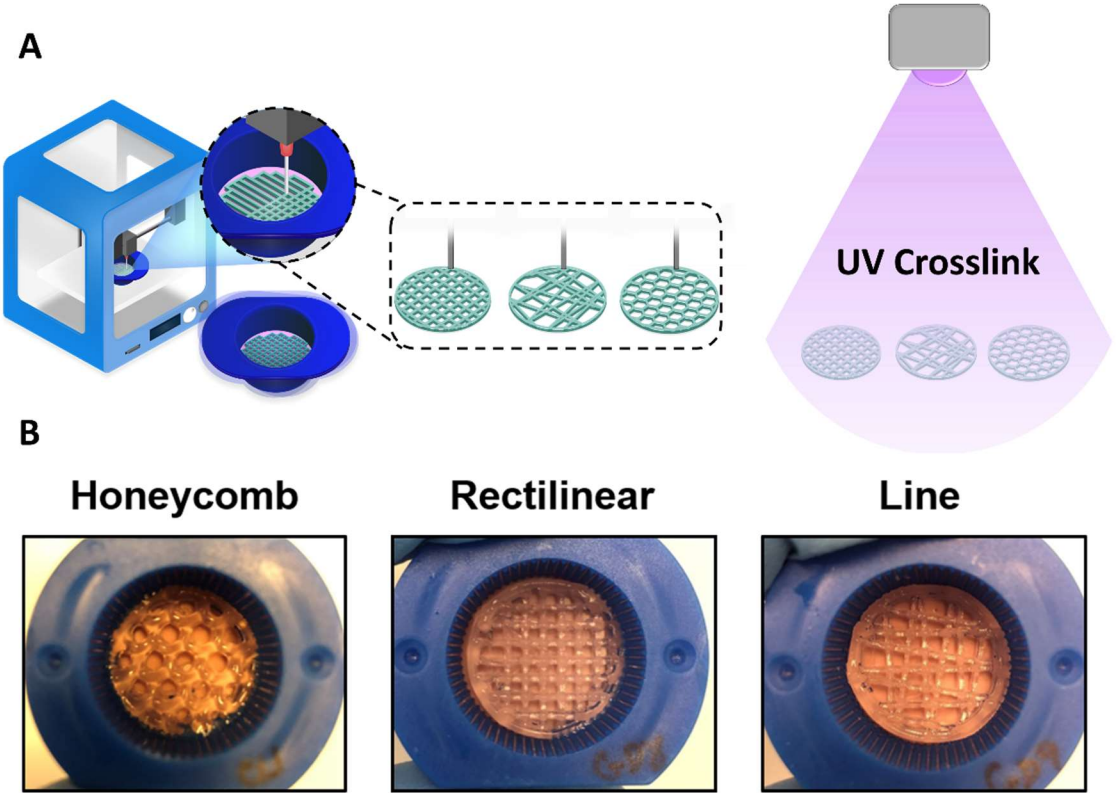

Figure 3-5 (A) Schematic explaining sample preparation – three different patterns were printed with PEGDA/Lap and UV crosslinked. (B) Honeycomb, rectilinear, and random line patterns printed with PEGDA/Lap at 20% infill density.

the patterns available in Slic3r software (see Figure 3-5). Samples were crosslinked for 5 minutes under UV light before measurement with the ElastoSens Bio^2.

3.1.8 Effect of bioprinting multiple materials in a scaffold on viscoelastic properties of a rectilinear scaffold

To determine the effect of 3D bioprinting a multi-material scaffold on the viscoelastic properties of a rectilinear scaffold, PEGDA/Lap and Alg/Lap were prepared and loaded into the two separate printheads on the Cellink Inkredible+ bioprinter. The G-code for

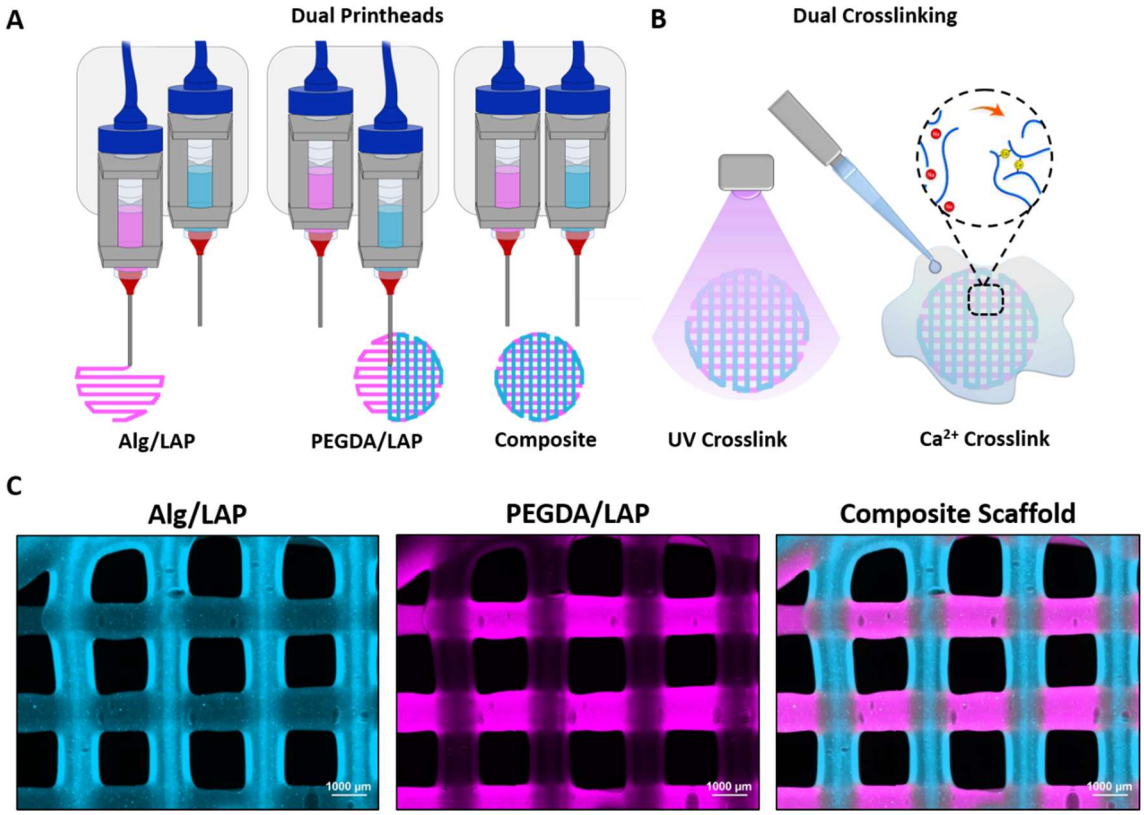

Figure 3-6 (A) A dual printhead system was used to print Alg/Lap and PEGDA/Lap into a composite rectilinear scaffold. (B) The scaffolds were first exposed to UV light to crosslink PEGDA/Lap and immersed in 2% $CaCl_2$ to crosslink Alg/Lap. (C) Multi-material 3D bioprinted rectilinear scaffold fluorescently labeled and imaged under the microscope (Scale bar = 1000µm).

printing the scaffold was prepared by manually editing the code for a rectilinear scaffold of one bioink in Repetier software. The code was post-processed using Cellink Heartware software to make it compatible with the Inkredible+ bioprinter. Alternating layers of each bioink were printed with the dual printhead system. The scaffold struts of each bioink were oriented perpendicularly (see Figure 3-6). The PEGDA/Lap bioink was crosslinked first with 5 minutes of exposure to UV light, and the Alg/Lap bioink was crosslinked second by filling in the scaffold with 2% $CaCl_2$ and crosslinking for 2 hours. PEGDA/Lap and Alg/Lap scaffolds with the same scaffold pattern and infill density were prepared and crosslinked with the same conditions for comparison. The samples were then analyzed using the ElastoSens Bio^2. The two bioinks were mixed with different coloured fluorescent microbeads and imaged using a fluorescent microscope to visualize the scaffold structure.

3.1.9 Statistical Analysis

All experiments were conducted in triplicate and the data were expressed as the mean ± standard deviation. Statistical analysis was conducted using two-way ANOVA on the appropriate experimental groups. P values < 0.05 were deemed as statistically different and p values < 0.01 were deemed extremely significant.

3.2 Results and Discussion

The developed method of characterization was carried out using microextrusion bioprinting with nanocomposite bioinks. Several proof-of-concept studies were conducted to exemplify the effectiveness of the method including studying the effect of fiber size and spacing in rectilinear scaffolds on mechanical properties, the effect of scaffold fiber size

on crosslinking time, the effect of infill density and scaffold pattern on mechanical properties, the effect of infill density on fluid uptake, the effect of bioink formulation on mechanical properties, and, finally, the effect of incorporating multiple materials into a 3D bioprinted scaffold on mechanical properties. Interesting results were found and will be discussed in this section.

As previously discussed, microextrusion bioprinting was chosen for this proof-of-concept for its ability to print higher viscosity inks through long needles, a requirement of the method proposed in chapter 2. The method of sample preparation was straight forward, however, the selection of a highly printable bioink was very helpful in this process. Both adherence to the sample cup silicone membrane and attachment to the sample cup wall are critical in obtaining accurate measurements. Degassing the bioink was an effective method of promoting adherence to the sample cup membrane. It is worth mentioning that this method of characterization, although it favours the microextrusion bioprinting technique, has potential for compatibility with other methods of 3D bioprinting. In this scenario, 3D bioprinted scaffolds may have to be printed outside of the sample cup and attached to the walls of the sample cup post-print. For this, the sample cup fixture prepared would be deemed unnecessary.

Alg/Lap rectilinear scaffolds of varying fiber size and fiber spacing were 3D bioprinted. These parameters were chosen to be expanded upon because rectilinear scaffolds are a common scaffold design due to their simple structure which can easily be altered to adjust porosity (Li *et al.*, 2005). Three scaffold of increasing fiber diameter with spacing held constant were printed and analyzed with the ElastoSens Bio^2. As shown in Figure 3-7,

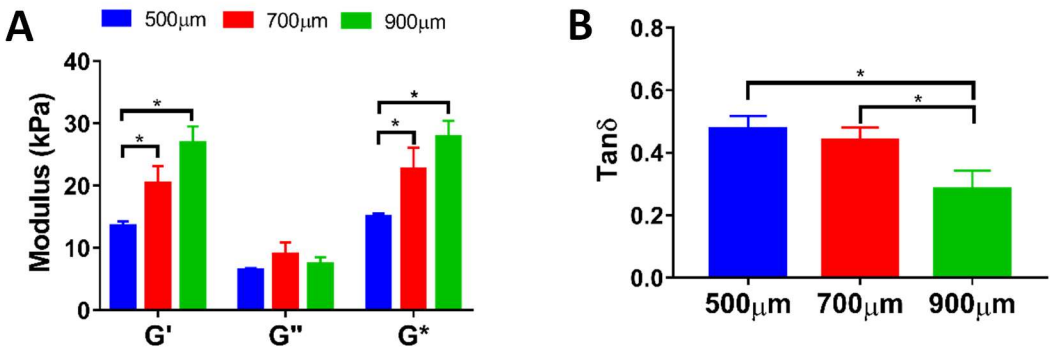

Figure 3-7 (A) the effect of fiber diameter on rectilinear Alg/Lap scaffold viscoelastic properties. (B) Decreasing Tanδ with increasing fiber diameter. *p<0.05

increasing fiber size resulted in an increasing G' which shows increasing mechanical strength of the scaffold with increasing fiber diameter. The G" did not display any measurable trend, likely due to there not being a large change in the overall liquid content of the scaffold with change in fiber size. The tanδ (loss factor), a ratio of G"/G' gives insight into the damping behaviour of viscoelastic materials (Sun *et al.*, 2013). A loss factor over 1 suggests more liquid like behaviour, whereas below 1 suggests more gel or solid like behaviour. The decreasing trend in the loss factor with increasing fiber diameter further supports the idea of increasing scaffold strength with increasing fiber size. Increasing the fiber spacing while maintaining constant fiber size yielded similar results. With increasing fiber spacing a decrease in G' was observed and no measurable trend in G", resulting in an increasing trend for the loss factor. Both experiments agree with the idea that increasing the porosity in a 3D bioprinted scaffold, either by decreased fiber sized or increased fiber spacing, results in a weakening of the mechanical strength of the structure and increased damping capability. This agrees with other results in the literature that have been generated

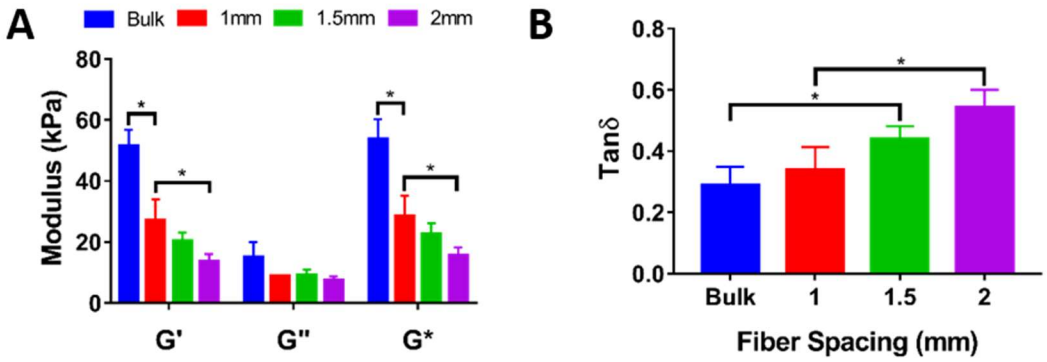

Figure 3-8 (A) Increased fiber spacing effects on the viscoelastic properties of rectilinear Alg/Lap scaffolds. (B) Increasing Tanδ with increasing fiber spacing. *p<0.05

for stiffer materials used in bone tissue engineering (Li *et al.*, 2005; Kelly *et al.*, 2018). It should be noted that the bulk material was also measured for this experiment and showed significantly increased mechanical strength in comparison to all the 3D bioprinted scaffolds.

As mentioned in chapter 1, altering the printed fiber size in scaffolds can influence diffusion of ions and biomolecules into the hydrogel. This effect was indirectly measured by analyzing the effect of fiber diameter on the ionic crosslinking time of Alg/Lap scaffolds. As shown in Figure 3-9, faster crosslinking time for 3D bioprinted scaffolds was shown by a plateau in the normalized G' around 45 minutes for 500 µm sized fibers and around 1 hour for the 900 µm fiber size. The bulk sample did not exhibit a plateau within the 2-hour time interval. These results were corroborated by imaging the diffusion of

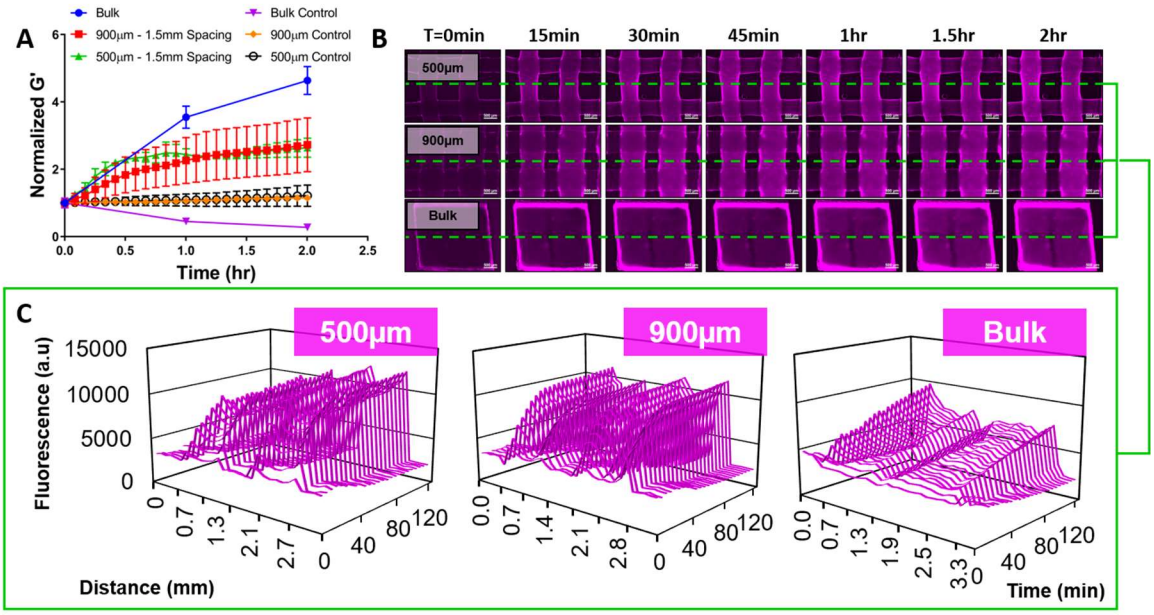

Figure 3-9 (A) Real-time crosslinking measurement of bulk Alg/Lap and 3D bioprinted scaffolds of with 900 and 500 µm fiber size. (B) Fluorescence images of rhodamine diffusing into samples over 2 hours (scale bar = 500µm). (C) Cross-sectional fluorescence of images above over 2 hours.

rhodamine, a fluorescent molecule, into the scaffolds and bulk material over the same time period. Similar plateaus were seen in the plotted cross-sectional fluorescence intensity for the 3D bioprinted samples. An increasing trend was still being observed at the 2-hour time point for the bulk sample. Both the 3D bioprinted scaffolds and the bulk control samples were treated with deionized water. They exhibited no increase in storage modulus due to the lack of crosslinker in solution. Interestingly, the bulk sample storage modulus decreased over the 2-hour time period; most likely an effect of material swelling. Swelling did not affect the storage moduli of the 3D bioprinted scaffolds due to their inherent macro-porosity. This type of real-time crosslinking analysis is possible only for the 3D bioprinted scaffolds due to the macro-porosity of the structures. Furthermore, a real time study such

as this would not be possible with traditional methods of mechanical properties characterization due to their destructive nature (Oyen, 2013; Roeder, 2013). A similar study of the crosslinking time may be possible with micro-rheology, in which micro-particle flow within a hydrogel is observed to determine rheological properties, however, this technique is only suitable for bulk materials and not 3D bioprinted scaffolds (Xia *et al.*, 2018). Hence, faster crosslinking times for 3D bioprinted structures would not be determined as was in this study. Another interesting result to notice is that the bulk material final G' value was ~4.5 times larger than its initial value, whereas both 3D bioprinted scaffolds were ~2.5 times larger than their initial values. This effect is likely due to the difference in overall volume of material in the samples.

For scaffolds which have non-rectilinear patterns, the infill density (a complementary term to porosity) is an adjustable scaffold design parameter that is often altered. PEGDA/Lap scaffolds were 3D bioprinted in a honeycomb pattern. Honeycomb scaffolds have been shown to be beneficial for many tissue types including heart, liver, and bone (George, Kuboki and Miyata, 2006; Tanaka *et al.*, 2006; Engelmayr Jr *et al.*, 2008). The

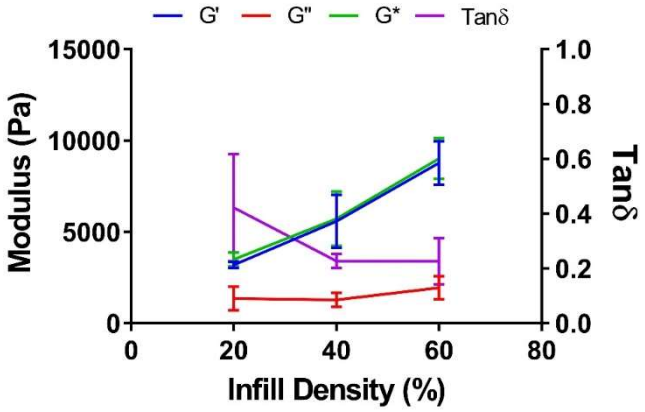

Figure 3-10 The effect of infill density on the viscoelastic properties of 3D bioprinted PEGDA/Lap honeycomb scaffolds.

infill density of the honeycomb pattern was 3D bioprinted at 20, 40, and 60%. Similarly to altering the porosity with fiber size and spacing, an increase in infill density, or decrease in porosity, resulted in an increase in the G' of the honeycomb scaffolds (see Figure 3-10). No measurable trend was observed in the G", resulting in a decreasing trend of the loss factor with increasing infill density. This experiment continues to support the notion that decreasing the porosity will result in an increase in mechanical strength and a decrease in damping capability. Similar results have been obtained in engineering intervertebral disks with a honeycomb scaffold, albeit a much stiffer material on the order of MPa (Hu *et al.*, 2018).

As mentioned in chapter 1, imposing porosity into a tissue scaffold by 3D bioprinting can improve nutrient, waste, and other biomolecule diffusion throughout the scaffold. 3D bioprinted PEGDA/Lap scaffolds were freeze-dried and employed in a swelling study to demonstrate this effect. This study did not require the use of the developed method; however, it supports the concepts that are being discussed about the usefulness of 3D bioprinting in tissue engineering. As shown in Figure 3-11, swelling occurred at a slightly faster rate for 3D bioprinted samples. However, there was no difference between the 3D

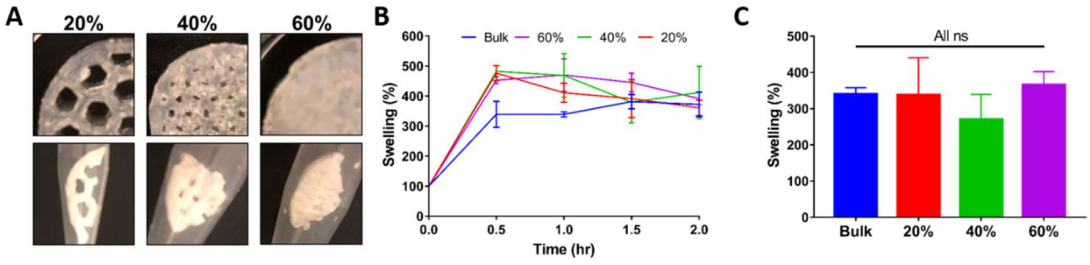

Figure 3-11 Summary of swelling study. (A) 3D bioprinted PEGDA/Lap scaffolds were freeze dried. (B) Swelling rate over 2 hours. (C) Final swelling after 6 hours showed no difference between scaffolds.

bioprinted samples because they were printed with the same fiber sizes. After 6 hours all samples showed no significant difference in swelling because they were all prepared from the same bioink. These results demonstrate improved interaction with the surrounding fluid environment in 3D bioprinted samples. This would allow for improved diffusion of nutrients, waste, and other biomolecules throughout the scaffold.

Another important step in the 3D bioprinting process is the determination of an optimal bioink formulation (Murphy and Atala, 2014). Often, the formulation is optimized to fine tune the bioink to a desirable stiffness to support tissue growth (Kolesky *et al.*, 2016; Zhao *et al.*, 2016). 2.5, 5, and 10% PEGDA with 6% Laponite bioinks were prepared and 3D bioprinted into honeycomb scaffolds with 20% infill density. As shown in Figure 3-12, increasing the concentration of the bioink resulted in an increase in G' or overall mechanical strength of the 3D bioprinted scaffolds. No measurable trend was observed for both the G" and loss factor. This observation is different than the previous studies where decreasing the macro-porosity has resulted in a decrease in the loss factor. This effect is

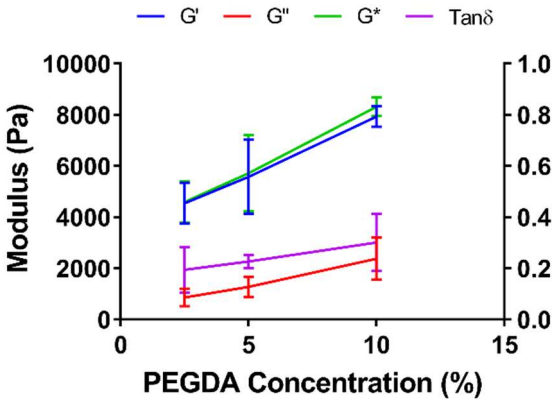

Figure 3-12 Effect of bioink concentration on viscoelastic properties of PEGDA/Lap honeycomb scaffold with constant infill density of 20%.

likely due to the scaffold structure remaining the same with only changes in in the bioink concentration.

In scaffold design, the printing pattern can play an important role for some tissue. Honeycomb scaffolds are often used for heart and liver tissues, and have been shown to exhibit higher strength with even distribution of stress throughout the scaffold (Tanaka *et al.*, 2006; Engelmayr Jr *et al.*, 2008; Lu *et al.*, 2015). A study of the effect of pattern on 3D bioprinted scaffolds using PEGDA/Lap was conducted with a rectilinear, honeycomb, and random line pattern. Honeycomb and rectilinear patterns were chosen for reasons previously mentioned, and the random line pattern was chosen to determine if large variance in interconnected pore size would have a detrimental effect on the mechanical strength. All patterns were printed with the same bioink formulation and infill density so that the only changing parameter was the pattern. As shown in Figure 3-13, the rectilinear and line patterns exhibited similar G' and G" values, whereas the honeycomb pattern was significantly higher for both G' and G". No significant difference was observed in the loss factors of each pattern. This was likely due to all three of the patterns having the same infill

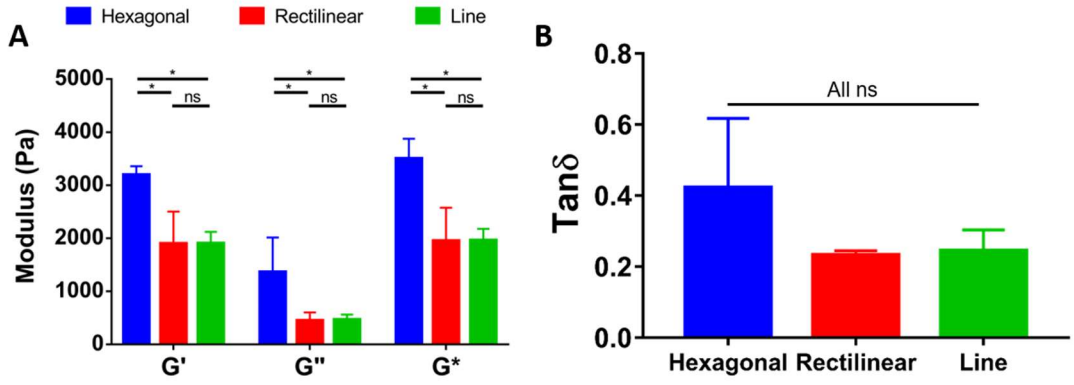

Figure 3-13 Effect of pattern on 3D bioprinted PEGDA/LAP scaffold (A) viscoelastic properties and (B) tanδ. *p<0.05

density. These results agree with another study which compared honeycomb and rectilinear patterned scaffolds for intervertebral disk regeneration using stiffer scaffolds in the order of MPa stiffness (Hu *et al.*, 2018).

Another common strategy in scaffold design is to 3D bioprint multi-material scaffolds with the intention of using the different materials for varying functions within the scaffold (Hong *et al.*, 2015; Rutz *et al.*, 2015). This strategy may be beneficial for cell and tissue growth, however, the effects on the mechanical strength of a scaffold are somewhat unpredictable. PEGDA/Lap and Alg/Lap were employed in 3D bioprinting a multi-material rectilinear scaffold with a two-step crosslinking method. Both the individual bioink scaffolds with the same structural parameters were also measured. Alg/Lap exhibited a much higher G' of 13 kPa compared to PEGDA/Lap at 2 kPa. The multi-material scaffold storage modulus was significantly different than both individual bioink samples, however, at 4kPa it was much closer to the PEGDA/Lap bioink scaffold G'. This suggests that the softer material had a higher influence in the overall mechanical strength

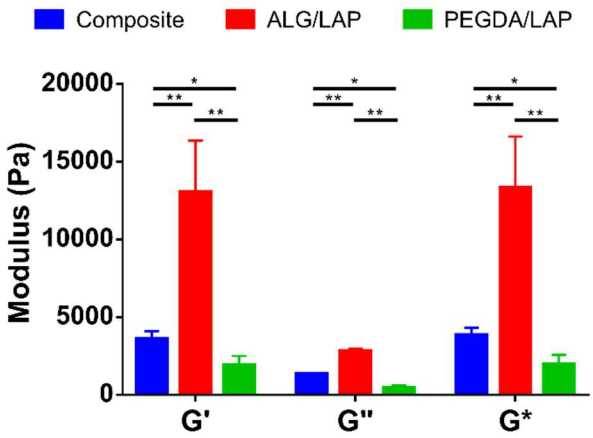

Figure 3-14 Viscoelastic properties of a multi-material rectilinear scaffold with Alg/Lap and PEGDA/Lap bioinks. *p<0.05, **p<0.01

of the multi-material scaffold. This can also be affected by a lack of crosslinking between the two bioinks. However, the results are interesting, and the method could prove very useful for engineering complex tissues with spatial arrangement of multiple materials and cell types.

3.3 Conclusion

The developed method of characterization, proposed in chapter 2 and determined to be effective in chapter 3, is capable of accurately measuring the effect of 3D bioprinted architectures on the mechanical properties of scaffolds for tissue engineering applications. As a proof of concept, several experiments were performed to demonstrate how the method of characterization would benefit development of 3D bioprinted hydrogel scaffolds for engineered tissues. Briefly, changing the porosity or infill density by varying parameters for rectilinear and honeycomb patterns was shown to have significant control in tuning the mechanical strength of scaffolds. Furthermore, the method is able to measure mechanical properties without contacting or destroying the sample, allowing for effective time-dependent studies. The was exemplified by a novel real-time ionic crosslinking study of 3D bioprinted Alg/Lap scaffolds. Simpler, but widely used ways of tuning mechanical properties, such as altering the bioink formulation can be effectively measured with this method as well. Interestingly, the effect of printing pattern was effectively shown to have a significant influence on the mechanical strength. This could prove very useful, for example, when using a set infill density while wanting to maximize mechanical strength. Finally, the method proves useful in measuring multi-material scaffolds. This has potential

to impact the forefront of the tissue engineering field in which inhomogeneous structures that effectively mimic complex tissue are being constructed.

Conclusion & Future Work

The field of tissue engineering has grown significantly since its inception in the late 1980s. There are many tissue engineered products now commercially available and generating revenue, or in clinical trials. However, the products that have reached commercialization are relatively simple in tissue structure. There is a significant need for improved ability to fabricate complex tissues that effectively mimic the native architecture of tissues found in the human body. Fulfillment of this need will push the field of tissue engineering from the research lab to the clinic.

3D bioprinting, an enabling technology, is seen as a promising tool for fast and effective fabrication of complex tissues which can recapitulate the spatial intricacies of native human tissues. The rise of this technology has spawned a new 3D bioprinting industry in which 3D bioprinters, bioinks, and 3D bioprinted products are all up for sale. As with many fast-growing, cutting-edge technologies, sometimes the capabilities of the technology move faster than the user or engineer knows how to effectively employ. 3D bioprinting offers a great deal of customizability in fabricating scaffolds for tissue engineering. There are four different 3D bioprinting techniques which all have their own advantages and ways of customizing fabricated scaffolds. Furthermore, the bioink itself has a great deal of customizability, and the architectural and compositional design of 3D bioprinted scaffolds is starting to be employed for further optimization of tissues.

With all this customizability, there is a need for better methods of characterization so that engineered tissues are totally optimized before moving to expensive animal testing and eventually clinical trials. Current strategy in optimizing the mechanical properties of soft

hydrogel 3D bioprinted tissue scaffolds is to characterize the bioink as a bulk material and fine tune it for cell attachment and growth. This strategy ignores the effect of 3D bioprinted architecture and scaffold design on the overall mechanical strength of the scaffold. When the engineered tissue is implanted *in vivo*, the scaffold is subject to the stresses of the local environment. A severe mismatch in mechanical integrity required for the implant can be a determining factor in the success of the engineered tissue.

This effect of 3D bioprinted architecture on mechanical strength has been investigated in the field of bone tissue engineering. This is due to the usefulness of compression testing for stiffer scaffold structures on the order of MPa to GPa. For softer hydrogel tissue scaffolds in the range of Pa to kPa, there are no effective methods of characterizing this effect in the literature. This further supports the need for an effective method of characterizing the effect of 3D bioprinted architecture and composition on scaffold mechanical strength.

In this thesis, a method of characterizing this effect using VeTBiM technology was proposed and further proven to be effective with several proof of concept experiments. For example, parameters which influence porosity, diffusion and fluid interaction with scaffolds, spatial arrangement of varying scaffold composition, and scaffold pattern were all shown to have significant effects on the mechanical strength of scaffolds using this method. Furthermore, non-destructive and contactless measurement allowed for real-time evaluation of crosslinking and indirect measurement of ion diffusion into the hydrogel scaffolds. To my knowledge, no such characterization has been demonstrated for 3D bioprinted soft hydrogel tissue scaffolds in the literature.

To further exemplify the potential impact of this method of characterization, an example will be discussed. Healthy myocardium is relatively soft and has a stiffness of 22-50kPa (Reis *et al.*, 2016). Engineered myocardial tissue for regeneration of infarct myocardium after suffering a heart attack presents a significant challenge in balancing mechanical stresses experienced in a beating heart with appropriate conditions for cell proliferation and tissue maturation. 3D bioprinting offers a useful platform with control over cell alignment to promote tissue contraction, as well as control over porosity to allow for nutrient diffusion, prevention of necrosis, and the formation of vasculature in the engineered tissue. However, the act of bioprinting a scaffold with controlled porosity weakens the overall mechanical strength of the structure, potentially nullifying the engineered tissue's effectiveness upon implantation. With the proposed and tested method, the mechanical strength, porosity, printed scaffold pattern, and cell alignment could all be optimized before going through with expensive animal testing and further on to clinical trials.

For future directions in this work, more temporal studies can be employed which involve tuning degradation rates with 3D bioprinting and growing cells on 3D bioprinted scaffolds. As tissues mature, cells secrete their own ECM proteins and enzymes that degrade some hydrogels. This process likely has an effect on the mechanical strength of an engineered tissue scaffold. The Gel/Lap bioink can be employed in this work due to its high level of biocompatibility and cell binding sites. Furthermore, employing this technique in optimizing an engineered tissue for a specific medical application would reinforce the developed method as an effective tool for *in vitro* optimization.

Bibliography

Agrawal, C. ., McKinney, J. ., Lanctot, D. and Athanasiou, K. . (2000) 'Effects of fluid flow on the in vitro degradation kinetics of biodegradable scaffolds for tissue engineering', *Biomaterials*. Elsevier, 21(23), pp. 2443–2452. doi: 10.1016/S0142-9612(00)00112-5.

Annual Regenerative Medicine Data Report (2018).

Atala, A., Kurtis Kasper, F. and Mikos, A. G. (2012) 'Engineering complex tissues', *Science Translational Medicine*, 4(160). doi: 10.1126/scitranslmed.3004890.

Au, P. I., Hassan, S., Liu, J. and Leong, Y. K. (2015) 'Behaviour of laponite gels: Rheology, ageing, pH effect and phase state in the presence of dispersant', *Chemical Engineering Research and Design*. Institution of Chemical Engineers, 101, pp. 65–73. doi: 10.1016/j.cherd.2015.07.023.

Avery, R. K., Albadawi, H., Akbari, M., Zhang, Y. S., Duggan, M. J., Sahani, D. V, Olsen, B. D., Khademhosseini, A. and Oklu, R. (2016) 'An injectable shear-thinning biomaterial for endovascular embolization', *Science Translational Medicine*, 8(365). doi: 10.1126/scitranslmed.aah5533.

Barr, S. W., Rodger, M. J. and Kelly, S. (2019) 'Developmental Perspective on Regenerative Medicine: An Update', *Science Insights*, 28(1), pp. 1–7. doi: 10.15354/si.19.re005.

Barsoum, R. G. S. (2015) *Elastomeric polymers with high rate sensitivity : applications in blast, shockwave, and penetration mechanics*.

Caliari, S. R. and Burdick, J. A. (2016) 'A practical guide to hydrogels for cell culture', *Nature Methods*. Nature Publishing Group, 13(5), pp. 405–414. doi: 10.1038/nmeth.3839.

Catros, S., Fricain, J.-C., Guillotin, B., Pippenger, B., Bareille, R., Remy, M., Lebraud, E., Desbat, B., Amédée, J. and Guillemot, F. (2011) 'Laser-assisted bioprinting for creating on-demand patterns of human osteoprogenitor cells and nano-hydroxyapatite', *Biofabrication*. IOP Publishing, 3(2), p. 025001. doi: 10.1088/1758-5082/3/2/025001.

Ceccaldi, C., Strandman, S., Hui, E., Montagnon, E., Schmitt, C., Hadj Henni, A. and Lerouge, S. (2017) 'Validation and application of a nondestructive and contactless method for rheological evaluation of biomaterials', *Journal of Biomedical Materials Research Part B: Applied Biomaterials*, 105(8), pp. 2565–2573. doi: 10.1002/jbm.b.33797.

Chen, Y., Zhou, S. and Li, Q. (2011) 'Microstructure design of biodegradable scaffold and its effect on tissue regeneration', *Biomaterials*. Elsevier, 32(22), pp. 5003–5014. doi: 10.1016/J.BIOMATERIALS.2011.03.064.

Chimene, D., Lennox, K. K., Kaunas, R. R. and Gaharwar, A. K. (2016) 'Advanced Bioinks for 3D Printing: A Materials Science Perspective', *Annals of Biomedical Engineering*, 44(6), pp. 2090–2102. doi: 10.1007/s10439-016-1638-y.

Chrisey, D. B., McGill, A. and Pique, A. (2000) 'Matrix assisted pulsed laser evaporation direct write'. Available at: https://patents.google.com/patent/US6766764B1/en

(Accessed: 6 July 2019).

Clarivate Analytics (2019a) *Acta Biomaterialia*, *InCites Journal Citation Reports*. Available at: https://apps-clarivate-com.ezproxy.library.uvic.ca/jif/home/?journal=ACTA BIOMATER&editions=SCIE&year=2017&pssid=J6-LdNedrIMZST2olxxxxzGotw9G1mZgIQ3yf-18x2dU8x2FKzMx2Fx2BaDeix2BC4bxxs5fRAx3Dx3DgS7nQIXZ4IYsx2BYG G6MzO9Qx3Dx3D-03Ff2gF3hTJGBPDScD1wSwx3Dx3D- (Accessed: 19 June 2019).

Clarivate Analytics (2019b) *Biomaterials*, *InCites Journal Citation Reports*. Available at: http://jcr.clarivate.com.ezproxy.library.uvic.ca/JCRJournalProfileAction.action?pg=JRNLPROF&journalImpactFactor=8.806&journalTitle=BIOMATERIALS&year=2017&edition=SCIE&journal=BIOMATERIALS (Accessed: 19 June 2019).

Clarivate Analytics (2019c) *Tissue Engineering*, *InCites Journal Citation Reports*. Available at: https://apps-clarivate-com.ezproxy.library.uvic.ca/jif/home/?journal=TISSUE ENG&editions=SCIE&year=2017&pssid=J6-LdNedrIMZST2olxxxxzGotw9G1mZgIQ3yf-18x2dU8x2FKzMx2Fx2BaDeix2BC4bxxs5fRAx3Dx3DgS7nQIXZ4IYsx2BYG G6MzO9Qx3Dx3D-03Ff2gF3hTJGBPDScD1wSwx3Dx3D-cLU (Accessed: 19 June 2019).

Cui, X., Gao, G., Yonezawa, T. and Dai, G. (2014) 'Human Cartilage Tissue Fabrication Using Three-dimensional Inkjet Printing Technology', *Journal of Visualized Experiments*, (88), p. e51294. doi: 10.3791/51294.

Derby, B. (2012) 'Printing and prototyping of tissues and scaffolds.', *Science (New York, N.Y.)*. American Association for the Advancement of Science, 338(6109), pp. 921–926. doi: 10.1126/science.1226340.

Discher, D. E., Mooney, D. J. and Zandstra, P. W. (2009) 'Growth factors, matrices, and forces combine and control stem cells.', *Science (New York, N.Y.)*. American Association for the Advancement of Science, 324(5935), pp. 1673–7. doi: 10.1126/science.1171643.

Engelmayr Jr, G. C., Cheng, M., Bettinger, C. J., Borenstein, J. T., Langer, R. and Freed, L. E. (2008) 'Accordion-like honeycombs for tissue engineering of cardiac anisotropy', *Nature Materials*, 7, pp. 1003–1010. doi: 10.1038/nmat2316.

Ferris, C. J., Gilmore, K. G., Wallace, G. G. and in het Panhuis, M. (2013) 'Biofabrication: an overview of the approaches used for printing of living cells', *Applied Microbiology and Biotechnology*. Springer-Verlag, 97(10), pp. 4243–4258. doi: 10.1007/s00253-013-4853-6.

Foyt, D. A., Norman, M. D. A., Yu, T. T. L. and Gentleman, E. (2018) 'Exploiting Advanced Hydrogel Technologies to Address Key Challenges in Regenerative Medicine', *Advanced Healthcare Materials*, 7(8). doi: 10.1002/adhm.201700939.

Gaharwar, A. K., Avery, R. K., Assmann, A., Paul, A., McKinley, G. H., Khademhosseini, A. and Olsen, B. D. (2014) 'Shear-Thinning Nanocomposite Hydrogels for the Treatment of Hemorrhage', *ACS Nano*. American Chemical Society, 8(10), pp.

9833–9842. doi: 10.1021/nn503719n.

George, J., Kuboki, Y. and Miyata, T. (2006) 'Differentiation of mesenchymal stem cells into osteoblasts on honeycomb collagen scaffolds', *Biotechnology and Bioengineering*. John Wiley & Sons, Ltd, 95(3), pp. 404–411. doi: 10.1002/bit.20939.

Gopinathan, J. and Noh, I. (2018) 'Recent trends in bioinks for 3D printing', *Biomaterials Research*. Biomaterials Research, 22(1), pp. 1–15. doi: 10.1186/s40824-018-0122-1.

Groll, J., Burdick, J. A., Cho, D.-W., Derby, B., Gelinsky, M., Heilshorn, S. C., Jüngst, T., Malda, J., Mironov, V. A., Nakayama, K., Ovsianikov, A., Sun, W., Takeuchi, S., Yoo, J. J. and Woodfield, T. B. F. (2018) 'A definition of bioinks and their distinction from biomaterial inks', *Biofabrication*. IOP Publishing, 11(1), p. 013001. doi: 10.1088/1758-5090/aaec52.

Gudapati, H., Dey, M. and Ozbolat, I. (2016) 'A comprehensive review on droplet-based bioprinting: Past, present and future', *Biomaterials*. Elsevier, 102, pp. 20–42. doi: 10.1016/J.BIOMATERIALS.2016.06.012.

Gungor-Ozkerim, P. S., Inci, I., Zhang, Y. S., Khademhosseini, A. and Dokmeci, M. R. (2018) 'Bioinks for 3D bioprinting: An overview', *Biomaterials Science*. Royal Society of Chemistry, 6(5), pp. 915–946. doi: 10.1039/c7bm00765e.

Hay, M., Thomas, D. W., Craighead, J. L., Economides, C. and Rosenthal, J. (2014) 'Clinical development success rates for investigational drugs', *Nature Biotechnology*, 32(1), pp. 40–51. doi: 10.1038/nbt.2786.

Henni, A. H. and Schmitt, C. (2019) 'System and method for measurements of viscoelastic parameters in soft materials'.

Henni, A. H., Schmitt, C. and Cloutier, G. (2010) 'Shear wave induced resonance elastography of soft heterogeneous media', *Journal of Biomechanics*. Elsevier Ltd, 43(8), pp. 1488–1493. doi: 10.1016/j.jbiomech.2010.01.045.

Hollister, S. J. (2005) 'Porous scaffold design for tissue engineering.', *Nature materials*, 4(7), pp. 518–24. doi: 10.1038/nmat1421.

Hong, S., Sycks, D., Chan, H. F., Lin, S., Lopez, G. P., Guilak, F., Leong, K. W. and Zhao, X. (2015) '3D Printing of Highly Stretchable and Tough Hydrogels into Complex, Cellularized Structures', *Advanced Materials*. John Wiley & Sons, Ltd, 27(27), pp. 4035–4040. doi: 10.1002/adma.201501099.

Hospodiuk, M., Dey, M., Sosnoski, D. and Ozbolat, I. T. (2017) 'The bioink: A comprehensive review on bioprintable materials', *Biotechnology Advances*. Elsevier Inc., 35(2), pp. 217–239. doi: 10.1016/j.biotechadv.2016.12.006.

Hu, D., Wu, D., Huang, L., Jiao, Y., Li, L., Lu, L. and Zhou, C. (2018) '3D bioprinting of cell-laden scaffolds for intervertebral disc regeneration', *Materials Letters*. North-Holland, 223, pp. 219–222. doi: 10.1016/J.MATLET.2018.03.204.

Hull, C. (1984) 'Apparatus for production of three-dimensional objects by stereolithography'. Available at: https://patents.google.com/patent/US4575330A/en (Accessed: 29 June 2019).

Instron Biomaterials - Instron (2019). Available at: http://www.instron.us/en-us/testing-solutions/by-material/biomaterials (Accessed: 4 July 2019).

Jackman, C. P., Ganapathi, A. M., Asfour, H., Qian, Y., Allen, B. W., Li, Y. and Bursac, N. (2018) 'Engineered cardiac tissue patch maintains structural and electrical properties after epicardial implantation', *Biomaterials*. Elsevier Ltd, 159, pp. 48–58. doi: 10.1016/j.biomaterials.2018.01.002.

Jakus, A. E., Rutz, A. L. and Shah, R. N. (2016) 'Advancing the field of 3D biomaterial printing', *Biomedical Materials (Bristol)*. IOP Publishing, 11(1). doi: 10.1088/1748-6041/11/1/014102.

Jin, Y., Liu, C., Chai, W., Compaan, A. and Huang, Y. (2017) 'Self-Supporting Nanoclay as Internal Scaffold Material for Direct Printing of Soft Hydrogel Composite Structures in Air', *ACS Applied Materials and Interfaces*, 9(20), pp. 17456–17465. doi: 10.1021/acsami.7b03613.

Jose, R. R., Rodriguez, M. J., Dixon, T. A., Omenetto, F. and Kaplan, D. L. (2016) 'Evolution of Bioinks and Additive Manufacturing Technologies for 3D Bioprinting', *ACS Biomaterials Science & Engineering*. American Chemical Society, 2(10), pp. 1662–1678. doi: 10.1021/acsbiomaterials.6b00088.

Kelly, C. N., Miller, A. T., Hollister, S. J., Guldberg, R. E. and Gall, K. (2018) 'Design and Structure–Function Characterization of 3D Printed Synthetic Porous Biomaterials for Tissue Engineering', *Advanced Healthcare Materials*, 7(7), pp. 1–16. doi: 10.1002/adhm.201701095.

Khademhosseini, A. and Langer, R. (2016) 'A decade of progress in tissue engineering', *Nature Protocols*, 11(10), pp. 1775–1781. doi: 10.1038/nprot.2016.123.

Kim, Y. S., Smoak, M. M., Melchiorri, A. J. and Mikos, A. G. (2018) 'An Overview of the Tissue Engineering Market in the United States from 2011 to 2018', *Tissue Engineering Part A*, 25(1–2), pp. 1–8. doi: 10.1089/ten.tea.2018.0138.

Klebe, R. J. (1988) 'Cytoscribing: A method for micropositioning cells and the construction of two- and three-dimensional synthetic tissues', *Experimental Cell Research*. Academic Press, 179(2), pp. 362–373. doi: 10.1016/0014-4827(88)90275-3.

Kloxin, A. M., Kloxin, C. J., Bowman, C. N. and Anseth, K. S. (2010) 'Mechanical properties of cellularly responsive hydrogels and their experimental determination', *Advanced Materials*, 22(31), pp. 3484–3494. doi: 10.1002/adma.200904179.

Kolesky, D. B., Homan, K. A., Skylar-Scott, M. A. and Lewis, J. A. (2016) 'Three-dimensional bioprinting of thick vascularized tissues', *Proceedings of the National Academy of Sciences*, 113(12), pp. 3179–3184. doi: 10.1073/pnas.1521342113.

Langer, R. and Vacanti, J. (1993) 'Tissue Engineering', *Science*, 260(5110), pp. 920–926.

Lee, J. M. and Yeong, W. Y. (2016) 'Design and Printing Strategies in 3D Bioprinting of Cell-Hydrogels: A Review', *Advanced Healthcare Materials*, 5(22), pp. 2856–2865. doi: 10.1002/adhm.201600435.

Li, J. P., de Wijn, J. R., van Blitterswijk, C. A. and de. Groot, K. (2005) 'Porous Ti6Al4V scaffolds directly fabricated by 3D fibre deposition technique: Effect of nozzle diameter', *Journal of Materials Science: Materials in Medicine*. Kluwer Academic Publishers, 16(12), pp. 1159–1163. doi: 10.1007/s10856-005-4723-6.

Lu, C., Zhao, M., Jie, L., Wang, J., Gao, Y., Cui, X. and Chen, P. (2015) 'Stress Distribution on Composite Honeycomb Sandwich Structure Suffered from Bending

Load', *Procedia Engineering*. Elsevier, 99, pp. 405–412. doi: 10.1016/J.PROENG.2014.12.554.

Malda, J., Visser, J., Melchels, F. P., Jüngst, T., Hennink, W. E., Dhert, W. J. A., Groll, J. and Hutmacher, D. W. (2013) '25th Anniversary Article: Engineering Hydrogels for Biofabrication', *Advanced Materials*. John Wiley & Sons, Ltd, 25(36), pp. 5011–5028. doi: 10.1002/adma.201302042.

Martínez Ávila, H., Schwarz, S., Rotter, N. and Gatenholm, P. (2016) '3D bioprinting of human chondrocyte-laden nanocellulose hydrogels for patient-specific auricular cartilage regeneration', *Bioprinting*. Elsevier, 1–2, pp. 22–35. doi: 10.1016/j.bprint.2016.08.003.

Miri, A. K., Khalilpour, A., Cecen, B., Maharjan, S., Shin, S.-R. and Khademhosseini, A. (2018) 'Multiscale Bioprinting of Vascularized Models', *Biomaterials*. Elsevier B.V. doi: 10.1016/j.biomaterials.2018.08.006.

Mironov, V., Reis, N. and Derby, B. (2006) 'Bioprinting: A Beginning', *Tissue Engineering*. Mary Ann Liebert, Inc. 2 Madison Avenue Larchmont, NY 10538 USA, 12(4), pp. 631–634. doi: 10.1089/ten.2006.12.631.

Murphy, S. V. and Atala, A. (2014) '3D bioprinting of tissues and organs', *Nature Biotechnology*. Nature Publishing Group, 32(8), pp. 773–785. doi: 10.1038/nbt.2958.

Ning, L. and Chen, X. (2017) 'A brief review of extrusion-based tissue scaffold bio-printing', *Biotechnology Journal*. John Wiley & Sons, Ltd, 12(8), p. 1600671. doi: 10.1002/biot.201600671.

O'Brien, F. J. (2011) 'Biomaterials & scaffolds for tissue engineering', *Materials Today*. Elsevier, 14(3), pp. 88–95. doi: 10.1016/S1369-7021(11)70058-X.

Odde, D. J. and Renn, M. J. (1999) 'Laser-guided direct writing for applications in biotechnology', *Trends in Biotechnology*. Elsevier Current Trends, 17(10), pp. 385–389. doi: 10.1016/S0167-7799(99)01355-4.

Olson, J. L., Atala, A. and Yoo, J. J. (2011) 'Tissue Engineering: Current Strategies and Future Directions', *Chonnam Medical Journal*, 47(1), p. 1. doi: 10.4068/cmj.2011.47.1.1.

Oyen, M. L. (2013) 'Mechanical characterisation of hydrogel materials', *International Materials Reviews*, 59(1), pp. 44–59. doi: 10.1179/1743280413y.0000000022.

Panwar, A. and Tan, L. P. (2016) 'Current status of bioinks for micro-extrusion-based 3D bioprinting', *Molecules*, 21(6). doi: 10.3390/molecules21060685.

Papanicolaou, G. C. and Zaoutsos, S. P. (2011) 'Viscoelastic constitutive modeling of creep and stress relaxation in polymers and polymer matrix composites', *Creep and Fatigue in Polymer Matrix Composites*. Woodhead Publishing, pp. 3–47. doi: 10.1533/9780857090430.1.3.

Parenteau, N. (1999) 'Skin: The First Tissue Engineered Products', *Scientific American*, pp. 83–85.

Peak, C. W., Stein, J., Gold, K. A. and Gaharwar, A. K. (2018) 'Nanoengineered Colloidal Inks for 3D Bioprinting', *Langmuir*, 34(3), pp. 917–925. doi: 10.1021/acs.langmuir.7b02540.

Pedde, R. D., Mirani, B., Navaei, A., Styan, T., Wong, S., Mehrali, M., Thakur, A.,

Mohtaram, N. K., Bayati, A., Dolatshahi-Pirouz, A., Nikkhah, M., Willerth, S. M. and Akbari, M. (2017) 'Emerging Biofabrication Strategies for Engineering Complex Tissue Constructs', *Advanced Materials*, 29(19), pp. 1–27. doi: 10.1002/adma.201606061.

Pereira, F. D. A. S., Parfenov, V., Khesuani, Y. D., Ovsianikov, A. and Mironov, V. (2018) 'Commercial 3D Bioprinters', *3D Printing and Biofabrication*, pp. 1–16. doi: 10.1007/978-3-319-40498-1_12-1.

Reis, L. A., Chiu, L. L. Y., Feric, N., Fu, L. and Radisic, M. (2016) 'Biomaterials in myocardial tissue engineering', *Journal of Tissue Engineering and Regenerative Medicine*. John Wiley & Sons, Ltd, 10(1), pp. 11–28. doi: 10.1002/term.1944.

Rheolution Inc. - Soft Materials Testing Instruments (2019). Available at: https://www.rheolution.com/ (Accessed: 26 June 2019).

Rider, P., Kačarević, Ž. P., Alkildani, S., Retnasingh, S. and Barbeck, M. (2018) 'Bioprinting of tissue engineering scaffolds.', *Journal of tissue engineering*. SAGE Publications, 9, p. 2041731418802090. doi: 10.1177/2041731418802090.

Roeder, R. K. (2013) 'Mechanical Characterization of Biomaterials', *Characterization of Biomaterials*. Academic Press, pp. 49–104. doi: 10.1016/B978-0-12-415800-9.00003-6.

Rutz, A. L., Hyland, K. E., Jakus, A. E., Burghardt, W. R. and Shah, R. N. (2015) 'A Multimaterial Bioink Method for 3D Printing Tunable, Cell-Compatible Hydrogels', *Advanced Materials*. Wiley-Blackwell, 27(9), pp. 1607–1614. doi: 10.1002/adma.201405076.

Soman, P., Chung, P. H., Zhang, A. P. and Chen, S. (2013) 'Digital microfabrication of user-defined 3D microstructures in cell-laden hydrogels', *Biotechnology and Bioengineering*. John Wiley & Sons, Ltd, 110(11), pp. 3038–3047. doi: 10.1002/bit.24957.

Sultan, S., Siqueira, G., Zimmermann, T. and Mathew, A. P. (2017) '3D printing of nano-cellulosic biomaterials for medical applications', *Current Opinion in Biomedical Engineering*. Elsevier Ltd, 2, pp. 29–34. doi: 10.1016/j.cobme.2017.06.002.

Sun, T. L., Kurokawa, T., Kuroda, S., Ihsan, A. Bin, Akasaki, T., Sato, K., Haque, M. A., Nakajima, T. and Gong, J. P. (2013) 'Physical hydrogels composed of polyampholytes demonstrate high toughness and viscoelasticity', *Nature Materials*. Nature Publishing Group, 12(10), pp. 932–937. doi: 10.1038/nmat3713.

Tanaka, M., Nishikawa, K., Okubo, H., Kamachi, H., Kawai, T., Matsushita, M., Todo, S. and Shimomura, M. (2006) 'Control of hepatocyte adhesion and function on self-organized honeycomb-patterned polymer film', *Colloids and Surfaces A: Physicochemical and Engineering Aspects*. Elsevier, 284–285, pp. 464–469. doi: 10.1016/J.COLSURFA.2005.11.098.

Vacanti, C. A. (2006) 'The history of tissue engineering', *Journal of Cellular and Molecular Medicine*. John Wiley & Sons, Ltd (10.1111), 10(3), pp. 569–576. doi: 10.1111/j.1582-4934.2006.tb00421.x.

Whitford, W. G. and Hoying, J. B. (2016) 'A bioink by any other name: terms, concepts and constructions related to 3D bioprinting.', *Future science OA*. Future Science Group, 2(3), p. FSO133. doi: 10.4155/fsoa-2016-0044.

Williams, D. F. (2014) 'The Biomaterials Conundrum in Tissue Engineering', *Tissue Engineering Part A*. Mary Ann Liebert, Inc. 140 Huguenot Street, 3rd Floor New Rochelle, NY 10801 USA , 20(7–8), pp. 1129–1131. doi: 10.1089/ten.tea.2013.0769.

Williams, D., Thayer, P., Martinez, H., Gatenholm, E. and Khademhosseini, A. (2018) 'A perspective on the physical, mechanical and biological specifications of bioinks and the development of functional tissues in 3D bioprinting', *Bioprinting*. Elsevier, 9, pp. 19–36. doi: 10.1016/J.BPRINT.2018.02.003.

Wilson, W. C. and Boland, T. (2003) 'Cell and organ printing 1: Protein and cell printers', *The Anatomical Record*. John Wiley & Sons, Ltd, 272A(2), pp. 491–496. doi: 10.1002/ar.a.10057.

Woodfield, T. B. F., Malda, J., De Wijn, J., Péters, F., Riesle, J. and Van Blitterswijk, C. A. (2004) 'Design of porous scaffolds for cartilage tissue engineering using a three-dimensional fiber-deposition technique', *Biomaterials*, 25(18), pp. 4149–4161. doi: 10.1016/j.biomaterials.2003.10.056.

Xia, Q., Xiao, H., Pan, Y. and Wang, L. (2018) 'Microrheology, advances in methods and insights', *Advances in Colloid and Interface Science*. Elsevier B.V., 257, pp. 71–85. doi: 10.1016/j.cis.2018.04.008.

Xu, L., Sheybani, N., Yeudall, W. A. and Yang, H. (2015) 'The effect of photoinitiators on intracellular AKT signaling pathway in tissue engineering application.', *Biomaterials science*. NIH Public Access, 3(2), pp. 250–5. doi: 10.1039/C4BM00245H.

Yousefzadeh, M. (2017) 'Modeling and simulation of the electrospinning process', *Electrospun Nanofibers*. Woodhead Publishing, pp. 277–301. doi: 10.1016/B978-0-08-100907-9.00012-X.

Zadpoor, A. A. (2017) 'Mechanics of additively manufactured biomaterials', *Journal of the Mechanical Behavior of Biomedical Materials*, 70, pp. 1–6. doi: 10.1016/j.jmbbm.2017.03.018.

Zhang, Y. S., Yue, K., Aleman, J., Mollazadeh-Moghaddam, K., Bakht, S. M., Yang, J., Jia, W., Dell'Erba, V., Assawes, P., Shin, S. R., Dokmeci, M. R., Oklu, R. and Khademhosseini, A. (2017) '3D Bioprinting for Tissue and Organ Fabrication', *Annals of Biomedical Engineering*, 45(1), pp. 148–163. doi: 10.1007/s10439-016-1612-8.

Zhao, X., Lang, Q., Yildirimer, L., Lin, Z. Y., Cui, W., Annabi, N., Ng, K. W., Dokmeci, M. R., Ghaemmaghami, A. M. and Khademhosseini, A. (2016) 'Photocrosslinkable Gelatin Hydrogel for Epidermal Tissue Engineering', *Advanced Healthcare Materials*, 5(1), pp. 108–118. doi: 10.1002/adhm.201500005.

Zhu, W., Ma, X., Gou, M., Mei, D., Zhang, K. and Chen, S. (2016) '3D printing of functional biomaterials for tissue engineering', *Current Opinion in Biotechnology*. Elsevier Ltd, 40, pp. 103–112. doi: 10.1016/j.copbio.2016.03.014.